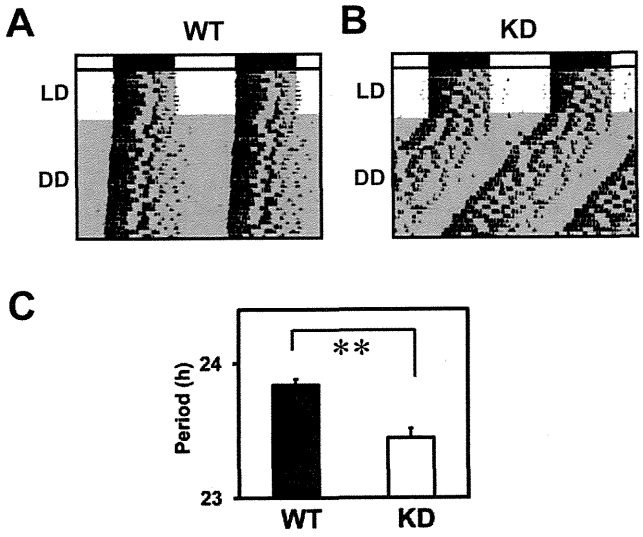

Figure 2. Short free-running period of locomotor activity rhythm in the KD mice. A, B, Locomotor activity rhythms of the WT (A) and KD (B) mice were entrained to 12:12 LD. But in DD, the KD mice exhibited circadian period of locomotor activity shorter than that of WTs. The vertical axis in each graph indicates the day path. Horizontal open and closed bars indicate the light and dark periods, respectively. **C,** The difference in the circadian period between the KD and WT mice (n = 15 each) was statistically significant $^{**}P<0.01$ vs. WT (Student's *t*-test).
doi:10.1371/journal.pone.0017655.g002

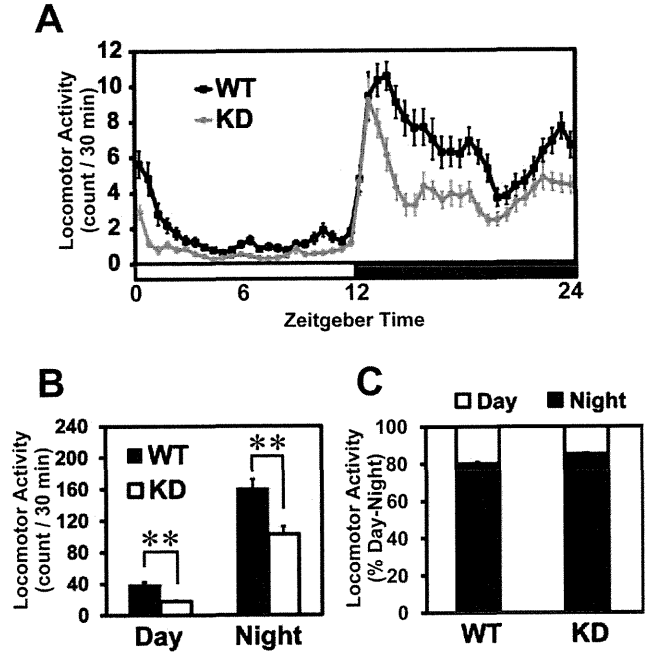

Figure 3. Reduced amount of locomotor activity in the *Rgs16* KD mice. A, Averaged daily activity plot of the KD and WT mice under LD condition. **B,** Average daytime or nighttime locomotor activity was significantly decreased in the KD mice as compared to that of WT controls (n = 21 each). $^{**}P<0.01$ vs. WT (Student's *t*-test). **C** Averaged day/night ratio of locomotor activity was comparable between the KD and WT mice (n = 21 each).
doi:10.1371/journal.pone.0017655.g003

Attenuated FAA in the *Rgs16* KD mice

The *Rgs16* mRNA in liver is not only circadianly regulated, but is also up-regulated by fasting and down-regulated by re-feeding [17]. These data raise the possibility that RGS16 is involved in metabolism in liver and in the food-driven behavior (FAA) regulated by a certain brain region(s) and/or liver. To test this, we next examined the effects of RF, daytime scheduled feeing for 4 hours (ZT6-ZT10), which is usually a resting period for nocturnal rodents. When mice are food-restricted during the day, FAA is observed about 3–4 hour prior to the feeding time [12]. In WT mice, a remarkable increase in the locomotor activities was observed for about 4 hours before the scheduled feeding time (Fig. 4A, C). On the other hand, the FAA of the KD mice was significantly attenuated in comparison with the controls (Fig. 4B, C). The reduction in the average percent FAA in the KD animals compared to that in the controls was statistically significant (Fig. 4D, $P<0.01$). Fig. 4E demonstrates FAA counts of individual KD and WT mice under RF as compared with baseline activity counts under free feeding (FF, as measured activity during ZT2-6). Bouts of locomotor activity during daytime was strongly reduced in KD group by RF, however, those in nighttime were comparable between WT and KD mice under FF or RF (Compare Fig. 3A and 4C). It is of note that, under the RF schedule, both WT and KD mice obtained almost the same amount of food during ZT6-ZT10 (0.88±0.08/10 g body weight/day for the WT; 0.80±0.05/10 g body weight/day for KD). Although body weight was slightly reduced by RF in both WT (33.1±2.8 g prior to and 30.0±1.6 g after RF) and KD mice (30.7±1.6 g prior to and 27.6±0.8 g after RF), there was no significant difference in the amount of food intake or the body weight between the two genotypes ($P>0.05$, Student's *t*-test).

Daytime-RF phase-advanced the *Per2* mRNA rhythm in WT, but not in KD

Reduced FAA has been reported in several knockout mice, but the mechanism underlying such behavioral change remains to be elucidated. To examine whether RF elicits FAA by affecting expression profiles of circadian clock gene and/or *Rgs16* in brain and liver, we sampled KD and WT mouse tissues at 4 time points (ZT5, 11, 17, and 23) and performed qPCR. Fig. 5 demonstrates the circadian rhythms in the *Per2* clock gene expression in liver and thalamus in both the WT and the KD mice, where *Rgs16* transcripts are abundantly expressed. Under FF, the *Per2* mRNA exhibited circadian rhythms both in liver ($F = 21.7$ $P<0.01$ for WT, $F = 16.1$ $P<0.05$ for KD, one-way ANOVA) and thalamus ($F = 5.1$ $P<0.05$ for WT) with a peak at ZT17 in both genotypes. Under RF in WTs, the *Per2* rhythms were significantly phase-advanced, peaking at ZT11 and ZT5 in liver and thalamus, respectively (Fig. 5A, C; $F = 25.2$ $P<0.01$ for liver, $F = 4.1$ $P<0.05$ for thalamus). In contrast, the phase of the *Per2* rhythms in the KD mice was unaffected by RF either in liver or thalamus (Fig. 5B, D).

Discussion

In the present study, we generated transgenic *Rgs16* KD mice using lentiviral vectors carrying a shRNA expression cassette and a modified microinjection method, i.e., perivitelline injection [27,28]. This gene silencing technique enabled us to efficiently generate sufficient numbers of transgenic mice within a few months, because of the higher rate of transgenesis by lentiviral vector injection compared with the conventional pronuclear DNA microinjection [29–31]. Moreover, this *in vivo* KD strategy could be a method of choice when disruption of the gene of interest is likely to cause lethality *in vivo*, or leads to a lack of phenotype because redundant functionalities from within the gene family or from related gene(s) result in compensation for the gene loss. We anticipated that *Rgs16* knockout could potentially be compensated by other *Rgs* genes (*Rgs2* and/or *Rgs4*), because these genes, which

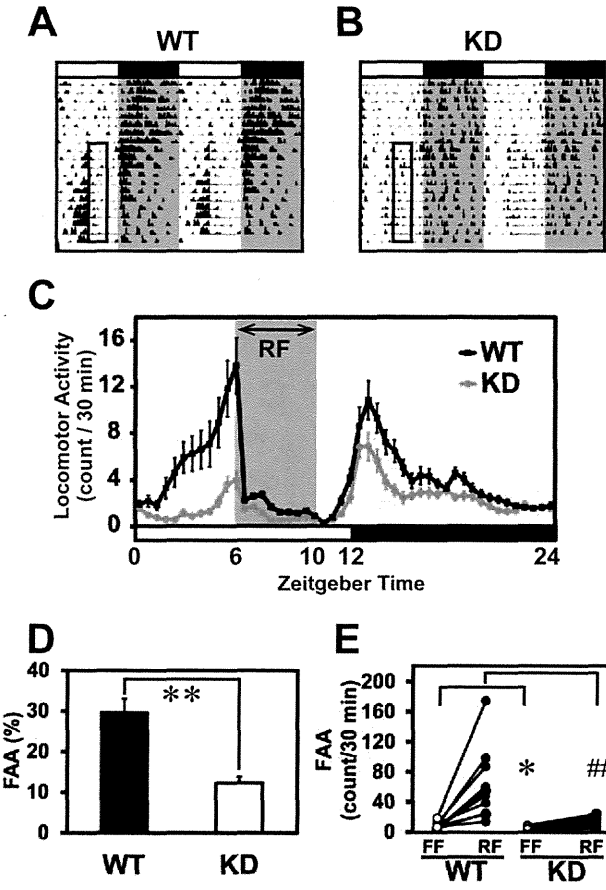

Figure 4. Attenuated FAA in the KD mice under daytime-RF. A, B, Examples of double-plotted actograms of WT (A) or KD (B) mice under RF. The RF time was set at ZT6–ZT10 (open box). Whereas WT mouse showed a strong FAA (A), those of KD were very weak (B). **C,** Averaged daily activity plot of the KD and WT mice under RF. **D,** Average percentages of FAA [100× activity counts (ZT2-6)/24-hour activity counts] during the last three days of RF between WT and KD mice were compared (n = 11 each). $^{**}P<0.01$ vs. WT (Student's *t*-test). **E,** FAA counts of individual mice during 4 hours preceding RF (ZT2-6) averaged over the first 7 days of FF and the following 12 days of RF were compared in each genotype (n = 11 each). $^{*}P<0.05$, vs. WT in FF; $\#\#P<0.01$ vs. WT in RF (Student's *t*-test).
doi:10.1371/journal.pone.0017655.g004

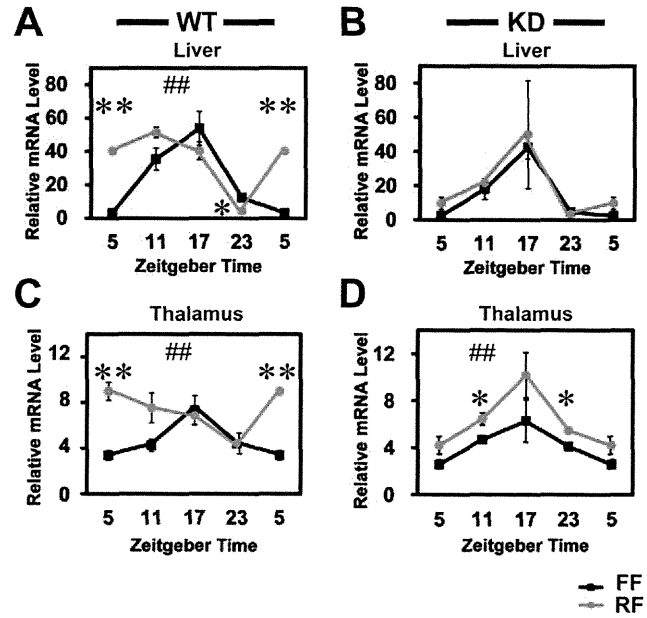

Figure 5. Daytime-RF phase-advanced circadian rhythms of *Per2* in liver and thalamus in WT, but not in the KD mice. Under RF (ZT6-10), the WT mice liver (**A**) and thalamus (**C**) phase-advanced *Per2* rhythms by 6 hours and 12 hours, respectively, as compared to the control mice under FF. In contrast, the circadian phase of *Per2* in the KD mice was not shifted in either liver (**B**) or thalamus (**D**) by RF. $\#\#P<0.01$ circadian gene expression profile by 2-way ANOVA (FF vs. RF mice, A, C, D). $^{**}P<0.01$, $^{*}P<0.05$ vs. WT (Student's *t*-test). n = 3–4 for each ZT point. FF, free feeding; RF, restricted feeding.
doi:10.1371/journal.pone.0017655.g005

belong to the same R4 subfamily along with *Rgs16*, are also circadianly expressed in the SCN [16]. Consistent with this expectation, another group reported no significant phenotype in the *Rgs16* knockout mice [32].

Our study provided evidence that G protein signaling modulated by RGS16 plays a role not only in the master LEO, but also in the FEO(s). Previous studies have indicated potential circadian roles of several GPCRs in the SCN. For instance, knockout and other studies strongly suggest that VIP and its receptor VPAC2, a member of GPCR family, are important for synchronization of the circadian clock and for sustaining circadian rhythmicity [18]. Likewise, GPCR ligands/GPCRs such as orexin/receptor and ghrelin/receptor are also involved in the FEO [23–26]. Further studies to identify upstream GPCR(s) will shed light on a significant role(s) of RGS16 in the SCN, thalamus and liver.

In the present study, expression level of *Per2* was up-regulated by RF, consistent with the previous report demonstrating an RF-induced change in basal level of gene expression [33]. Food seeking/satiety and energy metabolism may be one of the factors for FAA formation [23,24,34]. In addition, previous studies have shown that the volume of food can produce large phase-shifts in the FAA rhythm in rats, and also large phase-advance in the *Per2* gene expression in mouse liver in a food volume-dependent manner [35]. In our data, food availability and body weight change during RF conditions were not significantly different between the WT and KD mice, suggesting that deficit of FAA formation and phase-shift of the *Per2* expression in liver did not lead to impairment of food seeking ability and/or the digestive system. RGS16 is the first molecule that has been reported to control not only FAA formation but also phase-shift of liver clock by RF. Thus, our data could provide a new insight into where and how these signaling molecules including RGS proteins affect the circadian timing systems.

Our present study also demonstrated that, whereas the circadian rhythms of the *Per2* mRNA were significantly phase-advanced by daytime-RF, both in liver and thalamus compared to free-feeding WT controls, the *Per2* rhythms in the KD mice did not phase-shift in either organ. These results suggest that RGS16 is potentially an upstream regulator of the *Per2* rhythms in liver and thalamus, whereas expression of *Rgs16* itself is regulated by the circadian clock. The data also suggests that RGS16 is involved in the phase-shift of both behavioral and molecular rhythms evoked by RF. It is noteworthy that a phase-advance in the *Per2* rhythms by daytime-RF was observed in thalamus. These data, together with the specific expression of *Rgs16* in this brain region, imply that thalamus plays a role in the FEO. It has been reported that complete paraventricular thalamic nucleus (PVT) lesion affects LEO, but not FEO [36], although involvement of thalamic regions other than PVT in the circadian systems needs to be determined.

Interestingly, the report also indicated that PVT ablation increased total daily activity, suggesting that this thalamic region is involved in regulating behavioral output. Altogether, our data along with previous studies raise a possibility that RGS16 in thalamus modulates light-entrained and/or food-entrained behavior by regulating activity levels and/or circadian behavioral rhythms under different environmental conditions.

Our study provided for the first time evidence suggesting that two distinct regions of the body, thalamus and liver, where *Rgs16* mRNA is abundantly expressed, are involved in the regulation of the FAA under restricted food availability. The data raise the question of whether liver or thalamus plays a lead role in the FEO-operated FAA, or both of these regions regulate the behavior, either independently or cooperatively. Further studies in search of upstream GPCRs/ligands and downstream signaling molecules will elucidate the mechanism of how RGS16 specifically regulates food-entrained behavior in different loci.

Materials and Methods

Animals

C57BL/6J inbred mice were purchased from CREA Japan and used for generating transgenic mice and all other experiments. Animals were provided with food and water *ad libitum*, and entrained to 12 hr light: 12 hr dark condition (12:12 LD) for at least 2 weeks at 23±2°C, All animals were cared for in accordance with the Law (No. 105) and Notification (No. 6) of the Japanese Government, and all experiments were conducted under permission of the Experimental Animal Welfare Committees of Kinki University (Permission #KDMS-16-002) and Waseda University (Permission #08A36).

shRNA

Six shRNAs were designed from the *Rgs16* cDNA sequence, and annealed double-stranded oligomers were subcloned into the pSilencer 1.0-U6 siRNA Expression Vector (Ambion). Knockdown efficiencies of the expression vectors carrying individual shRNAs were evaluated by transient transfection of the vectors into mouse NIH3T3 (RIKEN Cell Bank) fibroblast cell line by Lipofectamine 2000 (Life Technologies) according to manufacturer's instruction. After 48 hours of incubation, cells were lysed using Sepazol-RNA I (Nacalai Tesque), RNA was extracted, and quantitative PCR (qPCR) was performed using *Rgs16* primers. Two shRNAs (#41, 53), which significantly suppressed the endogenous *Rgs16* expression levels, were used for transgenesis. The sequences of annealed oligonucleotides for expressing #41 or #53 shRNA were as follows:

#41: 5′-GCGAGGAGTTCAAGAAGATTTCAAGAGAATCTTCTTGAACTCCTCGCTTTTTT-3′ and 5′-AATTAAAAAAGCGAGGAGTTCAAGAAGATTCTCTTGAAATCTTCTTGAACTCCTCGCGGCC-3′

#53: 5′-GAGAACTGACCAAGACAAATTCAAGAGATTTGTCTTGGTCAGTTCTCTTTTTT-3′ and 5′-AATTAAAAAAGAGAACTGACCAAGACAAATCTCTTGAATTTGTCTTGGTCAGTTCTCGGCC-3′

Lentiviral vector construction and production of high-titer lentiviral vector particles

The two shRNA sequences (#41 and #53) targeting *Rgs16* along with the mouse U6 promoter were PCR-amplified from the pSilencer vectors and cloned into the pTZV TranzVector™ (Tranzyme) as depicted in Fig.S1. An eGFP fluorescent marker driven from the human immediate early cytomegalovirus virus (CMV) promoter is co-expressed with the shRNA hairpin sequence. High-titer lentiviral vector particles were generated using the Trans-Lentiviral™ Vector Packaging system [37]. Viral particles were concentrated by ultracentrifugation. Functional titers were determined by transducing HEK293T (ATCC) cells with limiting dilutions of virus and counting GFP-positive colonies.

Generation of *Rgs16* KD mice

Fertilized oocytes were harvested from super-ovulated C57BL/6J female mice. Viral vectors at a concentration of 1×10^9/ml were microinjected into the perivitelline space of the oocytes using a FemtoJet injector (Eppendorf), and then reimplanted into the oviduct of pseudo-pregnant recipient females after 2–4 hours of microinjection. Injections were performed under 400× magnification (DM IRE2, Leica), and injection volume was approximately 100 nl.

Genotyping and evaluation of the KD mice

For genotyping, genomic DNA was extracted from a tail tip of each mouse by a standard protocol using proteinase K and following phenol/chloroform extraction. Using the genomic DNA as a template, PCR was performed using GFP primers. To confirm expression of the GFP protein, we observed tail tips under fluorescent microscopy.

qPCR

Total RNA was extracted from tail tip, liver, and thalamus of each KD or WT control mouse using RNeasy Mini Kit (Qiagen). The extracted RNA was reverse-transcribed into cDNA using High Capacity cDNA Reverse Transcription Kit (Applied Biosystems). For qPCR reaction, SYBR GREEN Premix ExTaq (Takara) was used following manufacturer's instruction. The sequences of primers used in this study are as follows. GFP primers: 5′-AGCAAAGACCCCAACGAGA-3′ and 5′-GGCGGCGGTCACGAA-3′; *Rgs16* primers: 5′-TGCTTGTGAACAGGGCTAACTG-3′ and 5′-CTCCCTCCTTAGACCCCATCTT-3′; *Per2* primers: 5′-TGTGTCTTACACGGGTGTCCTA-3′ and 5′-ACGTTTGGTTTGCGCATGAA-3′, 18S rRNA primers: 5′-CGGCTACCACATCCAAGGAA-3′, 5′-GCTGGAATTACCGCGGCT-3′.

The value of the PCR product of the target gene was normalized to that of 18S rRNA.

Measurement of locomotor activity rhythm

Mice were individually housed in translucent polypropylene cages under 12:12 LD (200 lux) and DD, and locomotor activity was assessed either by a running wheel (Fig. 2) or an area sensor (F5B, Omron; Fig. 3, 4). Activity was continuously monitored and analyzed using ClockLab software (Actimetrics).

Schedules for RF

Individually housed KD mice and WT controls were maintained in a 12:12 LD cycle under FF for at least 7 days. The RF experiment for the measurement of anticipatory activity was performed as previously described [38]. Briefly, after 1 day of food deprivation starting at ZT12 (day 0), food was restricted to ZT6-ZT10 for 12 days (day 1–12). From day 13 to 14, food was again withdrawn for the entire day to record motor activity under food deprivation. Another RF experiment for the measurement of clock gene expression was performed. After application of the same RF conditions, animals were sacrificed at ZT5, 11, 17, and 23 on day 13 under food deprivation.

In situ hybridization (ISH)

Riboprobe was labeled with ^{35}S-UTP (Amersham/GE Healthcare) by *in vitro* transcription using either T7 or SP6 polymerase

(Promega). Frozen mouse brain sections (40 μm thickness) were hybridized with riboprobe for overnight and apposed to Kodak film (BioMax MR). The *Rgs16* cDNA (entire ORF length 606 bp) was amplified by PCR and subcloned into pGEM-T Easy Vector (Promega). The plasmids were linealized with *Nco*I to synthesize riboprobe.

Statistics

Results were expressed as the mean ± SEM. One-way ANOVA was applied to evaluate significant difference of circadian rhythmicity of gene expression, and 2-way ANOVA was applied to evaluate significance between KD and control mice. The significance of the differences between groups was determined by the Student's *t*-test. Statistical analysis software (StatView version 5.0, SAS Institute) was used.

Supporting Information

Figure S1 Schematic representation of the shRNA lentiviral vectors. The shRNA hairpin sequences (#41 and #53) targeting mouse *Rgs16* is cloned into pTZV, a HIV1-based self-inactivating (SIN) lentiviral transfer vector containing the central polypurine tract/termination sequence (FLAP) and the Woodchuck hepatitis virus post-transcriptional regulatory element (WPRE) for enhanced gene expression. A PCR-amplified fragment containing the mouse U6 promoter, shRNA hairpin, and pol III termination sequence (TTTTT) is cloned into pTZV between 5′ – *Cla*I and 3′ – *Bam*HI sites. A GFP marker is co-expressed with the shRNA from a CMV promoter to enable visualization of transduced cells and transgenic embryos.
(EPS)

Figure S2 *In vitro* knockdown of the *Rgs16* mRNA by shRNAs used in this study. 2 μg of the pSilencer 1.0 vector expressing either of the two shRNAs (#41 or #53) was transfected into the NIH3T3 mouse fibroblast cell line with Lipofectamine 2000. RNA was extracted from each of the transfected cells two days after the transfection, and expression levels of *Rgs16* were compared by qPCR (see Materials and Methods). Both #41 and #53 shRNAs significantly reduced the average *Rgs16* mRNA level (**$P<0.01$, $n=4$).
(EPS)

Acknowledgments

We thank Ralph Mistlberger for critical reading, and Takahiro Moriya, Yuka Miyoshi, Yuka Sugahara, Shinsuke Noso, Naru Babaya, Ikuko Yamada, Tomohiro Suzuki, Tamio Furuse and Hiroshi Takemori for technical support and helpful discussion.

Author Contributions

Conceived and designed the experiments: NH. Performed the experiments: NH KA SK SY STK KH. Analyzed the data: NH HI SW TM SS. Contributed reagents/materials/analysis tools: JKW RR MM. Wrote the paper: NH SS.

References

1. Lamont EW, James FO, Boivin DB, Cermakian N (2007) From circadian clock gene expression to pathologies. Sleep Med 8: 547–556.
2. Mendoza J (2007) Circadian clocks: setting time by food. J Neuroendocrinol 19: 127–137.
3. Dibner C, Schibler U, Albrecht U (2010) The mammalian circadian timing system: organization and coordination of central and peripheral clocks. Annu Rev Physiol 72: 517–549.
4. Schibler U, Ripperger J, Brown SA (2003) Peripheral circadian oscillators in mammals: time and food. J Biol Rhythms 18: 250–260.
5. Escobar C, Cailotto C, Angeles-Castellanos M, Delgado RS, Buijs RM (2009) Peripheral oscillators: the driving force for food-anticipatory activity. Eur J Neurosci 30: 1665–1675.
6. Krieger DT, Hauser H, Krey LC (1977) Suprachiasmatic nuclear lesions do not abolish food-shifted circadian adrenal and temperature rhythmicity. Science 197: 398–399.
7. Rashotte ME, Stephan FK (1996) Coupling between light- and food-entrainable circadian oscillators in pigeons. Physiol Behav 59: 1005–1010.
8. Stephan FK (2001) Food-entrainable oscillator in mammals. Circadian Clocks 12: 223–246.
9. Stephan FK, Swann JM, Sisk CL (1979) Entrainment of circadian rhythms by feeding schedules in rats with suprachiasmatic lesions. Behav Neural Biol 25: 545–554.
10. Stephan FK, Swann JM, Sisk CL (1979) Anticipation of 24-hr feeding schedules in rats with lesions of the suprachiasmatic nucleus. Behav Neural Biol 25: 346–363.
11. Challet E, Mendoza J, Dardente H, Pevet P (2009) Neurogenetics of food anticipation. Eur J Neurosci 30: 1676–1687.
12. Mistlberger RE (1994) Circadian food-anticipatory activity: formal models and physiological mechanisms. Neurosci Biobehav Rev 18: 171–195.
13. Mistlberger RE (2009) Food-anticipatory circadian rhythms: concepts and methods. Eur J Neurosci 30: 1718–1729.
14. Willars GB (2006) Mammalian RGS proteins: multifunctional regulators of cellular signalling. Semin Cell Dev Biol 17: 363–376.
15. Grafstein-Dunn E, Young KH, Cockett MI, Khawaja XZ (2001) Regional distribution of regulators of G-protein signaling (RGS) 1, 2, 13, 14, 16, and GAIP messenger ribonucleic acids by in situ hybridization in rat brain. Brain Res Mol Brain Res 88: 113–123.
16. Ueda HR, Chen W, Adachi A, Wakamatsu H, Hayashi S, et al. (2002) A transcription factor response element for gene expression during circadian night. Nature 418: 534–539.
17. Huang J, Pashkov V, Kurrasch DM, Yu K, Gold SJ, et al. (2006) Feeding and fasting controls liver expression of a regulator of G protein signaling (Rgs16) in periportal hepatocytes. Comp Hepatol 5: 8.
18. Maywood ES, O'Neill JS, Chesham JE, Hastings MH (2007) Minireview: The circadian clockwork of the suprachiasmatic nuclei–analysis of a cellular oscillator that drives endocrine rhythms. Endocrinology 148: 5624–5634.
19. Hannibal J (2002) Neurotransmitters of the retino-hypothalamic tract. Cell Tissue Res 309: 73–88.
20. Gillette MU, Mitchell JW (2002) Signaling in the suprachiasmatic nucleus: selectively responsive and integrative. Cell Tissue Res 309: 99–107.
21. Pevet P, Agez L, Bothorel B, Saboureau M, Gauer F, et al. (2006) Melatonin in the multi-oscillatory mammalian circadian world. Chronobiol Int 23: 39–51.
22. Dubocovich ML (2007) Melatonin receptors: role on sleep and circadian rhythm regulation. Sleep Med 8(Suppl 3): 34–42.
23. Akiyama M, Yuasa T, Hayasaka N, Horikawa K, Sakurai T, et al. (2004) Reduced food anticipatory activity in genetically orexin (hypocretin) neuron-ablated mice. Eur J Neurosci 20: 3054–3062.
24. Mieda M, Williams SC, Sinton CM, Richardson JA, Sakurai T, et al. (2004) Orexin neurons function in an efferent pathway of a food-entrainable circadian oscillator in eliciting food-anticipatory activity and wakefulness. J Neurosci 24: 10493–10501.
25. LeSauter J, Hoque N, Weintraub M, Pfaff DW, Silver R (2009) Stomach ghrelin-secreting cells as food-entrainable circadian clocks. Proc Natl Acad Sci U S A 106: 13582–13587.
26. Blum ID, Patterson Z, Khazall R, Lamont EW, Sleeman MW, et al. (2009) Reduced anticipatory locomotor responses to scheduled meals in ghrelin receptor deficient mice. Neuroscience 164: 351–359.
27. Lois C, Hong EJ, Pease S, Brown EJ, Baltimore D (2002) Germline transmission and tissue-specific expression of transgenes delivered by lentiviral vectors. Science 295: 868–872.
28. Shaughnessy L, Chamblin B, McMahon L, Nair A, Thomas MB, et al. (2004) Novel approaches to models of Alzheimer's disease pathology for drug screening and development. J Mol Neurosci 24: 23–32.
29. Park F (2007) Lentiviral vectors: are they the future of animal transgenesis? Physiol Genomics 31: 159–173.
30. Singer O, Verma IM (2008) Applications of lentiviral vectors for shRNA delivery and transgenesis. Curr Gene Ther 8: 483–488.
31. Gama Sosa MA, De Gasperi R, Elder GA (2010) Animal transgenesis: an overview. Brain Struct Funct 214: 91–109.
32. Bansal G, Druey KM, Xie Z (2007) R4 RGS proteins: regulation of G-protein signaling and beyond. Pharmacol Ther 116: 473–495.
33. Oishi K, Kasamatsu M, Ishida N (2004) Gene- and tissue-specific alterations of circadian clock gene expression in streptozotocin-induced diabetic mice under restricted feeding. Biochem Biophys Res Commun 317: 330–334.
34. Stephan FK (1997) Calories affect zeitgeber properties of the feeding entrained circadian oscillator. Physiol Behav 62: 995–1002.

35. Hirao A, Tahara Y, Kimura I, Shibata S (2009) A balanced diet is necessary for proper entrainment signals of the mouse liver clock. PLoS One 4: e6909.
36. Landry GJ, Yamakawa GR, Mistlberger RE (2007) Robust food anticipatory circadian rhythms in rats with complete ablation of the thalamic paraventricular nucleus. Brain Res 1141: 108–118.
37. Wu X, Wakefield JK, Liu H, Xiao H, Kralovics R, et al. (2000) Development of a novel trans-lentiviral vector that affords predictable safety. Mol Ther 2: 47–55.
38. Wakamatsu H, Yoshinobu Y, Aida R, Moriya T, Akiyama M, et al. (2001) Restricted-feeding-induced anticipatory activity rhythm is associated with a phase-shift of the expression of mPer1 and mPer2 mRNA in the cerebral cortex and hippocampus but not in the suprachiasmatic nucleus of mice. Eur J Neurosci 13: 1190–1196.

Bioconjugate Chemistry

ARTICLE

pubs.acs.org/bc

Fluorescence-Quenching Screening of Protein Kinase C Ligands with an Environmentally Sensitive Fluorophore

Wataru Nomura,[†] Nami Ohashi,[†] Yoshiaki Okuda,[†,‡] Tetsuo Narumi,[†] Teikichi Ikura,[‡] Nobutoshi Ito,[‡] and Hirokazu Tamamura*[,†,‡]

[†]Department of Medicinal Chemistry, Institute of Biomaterials and Bioengineering, Tokyo Medical and Dental University, 2-3-10 Kandasurugadai, Chiyoda-ku, Tokyo 101-0062, Japan

[‡]Graduate School of Biomedical Science, Tokyo Medical and Dental University, 1-5-45 Yushima, Bunkyo-ku, Tokyo 113-8510, Japan

Supporting Information

ABSTRACT: A novel fluorescence-quenching screening method for protein kinase C (PKC) ligands was developed utilizing solvatochromic fluorophores. Solvatochromic dyes, highly sensitive to the presence or the absence of competitive ligands in their binding to the C1b domain of PKCδ (δC1b), were combined with a known pharmacophoric moiety of 1,2-diacylglycerol (DAG) lactones, PKC ligands. Addition of δC1b to the fluorescent compounds caused a gradual increase in the fluorescent intensity in proportion to the increase of δC1b. As a competitive ligand was added to the complex of δC1b domain and fluorescent compounds, a gradual decrease in the fluorescent intensity was observed. The relative binding affinities of known ligands were successfully determined by this fluorescent method and corresponded well to the K_i values measured by a radioisotope method. These results indicate that washing, which is a laborious step in binding evaluations, is not required for this environmentally sensitive fluorophore based system. Screening with the system was performed for 2560 preselected library compounds with possible pharmacophores, and some lead compounds were found. This fluorescence-based method could be applied widely to known ligand−receptor combinations.

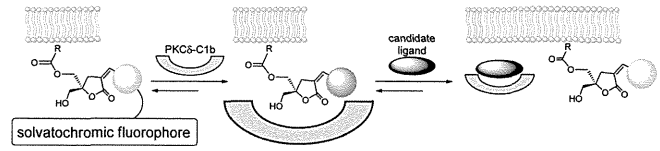

INTRODUCTION

Solvatochromic fluorophores are sensitive to immediate changes in their environment such as binding of ligands to proteins,[1] and significant biological issues have been examined by chemical probes with fluorescent dyes.[2,3] The major advantage of the fluorescence-based methods in the observation of physiological phenomena in cells is that detection and evaluation can be performed in real-time directly by microscopy. In these techniques, the signal/background ratio is critical to avoid the observation of artifacts or to obtain clearer images at high resolution. Screening methods of bioactive compounds have been developed as another application of fluorescence.[4] From the aspect of sensitivity, radioisotope (RI) based methods are more efficient but involve laborious experimental procedures. For the development of convenient screening procedures, a simple method for evaluation of binding is needed. By attachment of solvatochromic fluorophores to known ligands, the binding affinity of unknown ligands can be evaluated and related to RI methods.[5] Fluorescent intensity is highly dependent on the binding state to a target protein, and the signal/background ratio would be sufficient without washing steps, which are normally necessary in fluorescent analysis.[6,7]

In this study, we have developed reporter compounds containing solvatochromic dyes for the detection of ligand binding to a target protein and applied them to the screening of chemical libraries. Protein kinase Cδ (PKCδ) was chosen as a target protein because of its importance in physiological phenomena. The 11 isozymes that constitute PKC play pivotal roles in physiological responses to growth factors, oxidative stress, 1,2-diacylglycerol (DAG), and tumor promoters, such as phorbol esters. These responses regulate numerous cellular processes,[8,9] including proliferation,[10] differentiation,[11] migration,[12] and apoptosis.[13,14] Membrane translocation of PKC is caused by binding of ligands to the C1b domain and has been recognized as an important phenomenon in signal transduction because the localization of PKC is key in determining isozyme-specific functions by defining binding partners for downstream signaling.[15] Despite the complex regulatory mechanisms of PKC activation, considerable progress has been made in understanding isozyme-specific functions[16] and several ligands with high specificity for PKC isozymes have been developed as potential drugs.[17−23] Through the development of DAG-lactones, whose design is based on the endogenous ligand DAG, the importance of maintaining intact the pharmacophore triad of two carbonyl groups (*sn*-1 and *sn*-2) and the primary alcohol has been established as a requirement in high affinity ligands for PKC (Figure 1).[16] Various PKC ligands have been synthesized and found to be inhibitors of tumor promotion or of other diseases.

Received: December 13, 2010
Revised: March 13, 2011
Published: March 25, 2011

ACS Publications © 2011 American Chemical Society

However, there are limitations to the design of compound templates so far. Thus, in this study, we have attempted to develop the screening methods aimed at discovery of novel template structures for PKCδ ligands as drug leads.

EXPERIMENTAL PROCEDURES

General. ^{1}H NMR spectra were recorded using a Bruker AV500 spectrometer. Chemical shifts were reported in δ (ppm) relative to Me_4Si (in $CDCl_3$) as an internal standard. Low- and high-resolution mass spectra were recorded on a JMS-T1000LC AccuTOF and Bruker Daltonics microTOF-2focus in both positive and negative detection modes. Wakogel C-200 (Wako Pure Chemical Industries, Ltd.) and silica gel 60 N (Kanto Chemical Co., Inc.) were employed for flash chromatography. Fluorescent spectra were recorded on a JASCO FP-6600 spectrofluorometer and JASCO V-650 spectrophotometer using a quartz cell with 1.0 cm path length. Fluorescent intensities of samples in 96-well plates were recorded on Wallac ARVO MX.

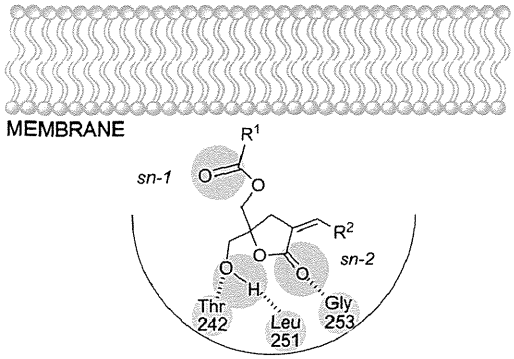

Figure 1. Binding mode of DAG-lactone derivatives to the δC1b domain. The *sn*-1 and *sn*-2 carbonyl groups are indicated. Three important pharmacophores are indicated by light blue spheres. Amino acid residues interacting with these pharmacophores (threonine at 242, leucine at 251, and glycine at 253) are indicated by red spheres.

Standard Monoacylation Procedure. Under argon, Et_3N (3 equiv) was added at 0 °C to a solution containing 5,5-bis(hydroxymethyl)oxalan-2-one in THF, and the mixture was stirred at 0 °C for 30 min. Then 0.2−1.1 equiv of a carboxylic acid derivative (an acyl chloride or carboxylic anhydride) was added. This mixture was stirred at 0 °C for a further 4 h. After evaporation of the solvent, the obtained residue was purified by flash column chromatography.

Preparation of Compounds 7, 10−13, 16, 17, and 19−21. Compounds **7**, **10**−**12**, and **16** were prepared as described in ref 17. Compounds **13** and **17** were prepared as described in refs 24 and 25. The synthesis of **19** is described elsewhere.[26] Compounds **20** and **21** are commercially available.

Expression and Purification of the δC1b Domain. DNA coding C1b domain of mouse PKCδ (231−280)[27] was subcloned into *Bam*H1 and *Eco*RI sites of pGEX-2tk (GE Healthcare) and expressed as gluthatione-*S*-transferase (GST) fusion protein in *Escherichia coli* C41 which contains extension sequences Gly-Ser-Arg-Arg-Ala-Ser-Val-Gly-Ser and Glu-Phe-Ile-Val-Thr-Asp at the N- and C-termini, respectively. The δC1b

Scheme 1. Synthesis of Fluorescent Compounds 1−3[a]

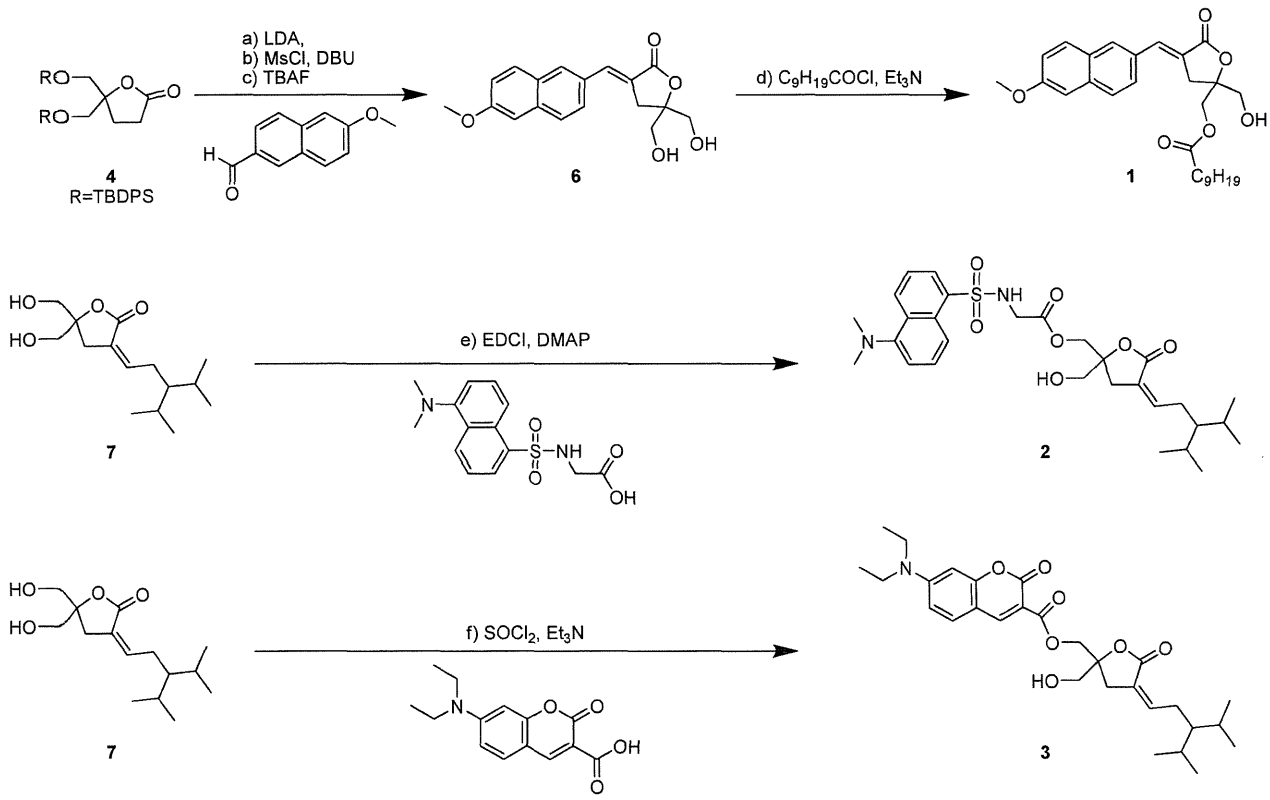

[a] (a) LDA, −78 °C; (b) MsCl, DBU, 0 °C to room temp; (c) TBAF, 0 °C to room temp; (d) $C_9H_{19}COCl$, Et_3N, 0 °C; (e) EDCI, DMAP, 0 °C; (f) $SOCl_2$, Et_3N, 0 °C.

dx.doi.org/10.1021/bc100567k |*Bioconjugate Chem.* 2011, 22, 923–930

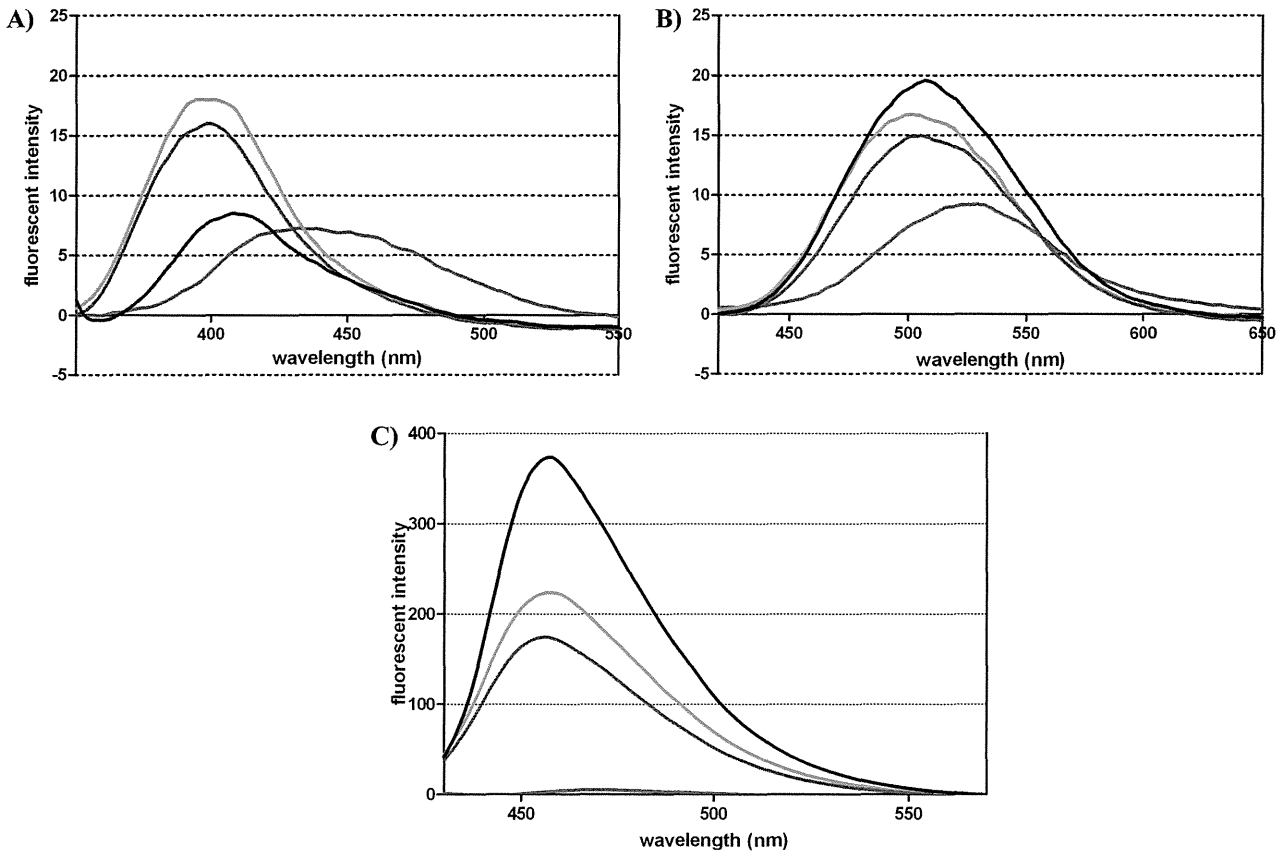

Figure 2. Fluorescent spectra of compounds **1** (A), **2** (B), and **3** (C) in different solvents. The spectra show fluorescence in the solvents color-coded as follows: red, MeOH; blue, THF; black, $CHCl_3$; green, EtOAc. Each ligand was prepared as 1 mM solution in DMSO. In UV measurement, 10 μL of ligand was added to 990 μL of solvents.

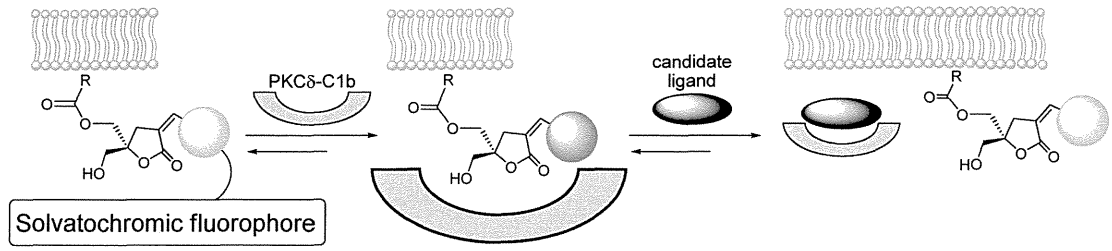

Figure 3. Schematic representation of a fluorescence-quenching screening system. In the presence of the δC1b domain, fluorescence of a solvatochromic fluorophore is enhanced. The replacement by candidate compounds results in fluorescence quenching.

Table 1. Changes of Fluorescent Intensity upon δC1b Binding and Inhibition Constants to δC1b Determined by Competition Assay against [^{3}H]PDBu

compd	ΔF[a]	K_i (nM)[b]
1	3.8	35.9
2	2.3	368
3	0.50	93.3

[a] Fluorescent change by binding of the δC1b domain. The values were determined by titration of the δC1b domain. The ΔF was determined by dividing F_1 by F_0 at the maximum of fluorescent emission in each spectrum. [b] Inhibitory constants determined by competition analysis against [^{3}H]PDBu.[28,36,37]

domain after cleavage contains 65 amino acid residues. Cells were grown at 37 °C in LB medium and induced with 0.3 mM IPTG at growth phase. Cells were cultured overnight at 20 °C after induction. Cells were collected and lysed in 50 mM Tris·HCl buffer (pH 8.0) containing 100 mM NaCl, 1 μg/mL leupeptine, 1 mM PMSF, and 1 mM DTT. Expressed protein was extracted by sonication, then purified by affinity chromatography utilizing glutathione-Sepharose 4B beads resin. GST moiety was cleaved by 300 units of thrombin at 4 °C overnight. The cleaved protein was eluted and further purified on a 2.6 cm × 60 cm Superdex S-75 gel filtration column. Purification was by FPLC system at a flow rate of 1 mL/min utilizing 0.1 M triethanolamine·HCl (pH 7.0) containing 0.5 M NaCl.

dx.doi.org/10.1021/bc100567k |*Bioconjugate Chem.* 2011, 22, 923–930

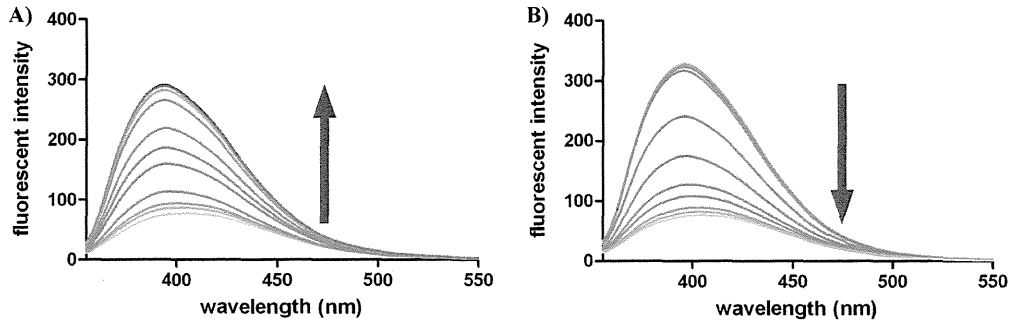

Figure 4. Changes of fluorescent spectra of compound **1** during titration of the δC1b domain (A) and during titration of PDBu (compound **8**) (B) after δC1b binding. The concentration of the δC1b domain was increased to 1.28 μM (6.4 equiv to compound **1**) by titration. The concentration of PDBu was increased to 10.2 μM (51.2 equiv to compound **1**) by titration.

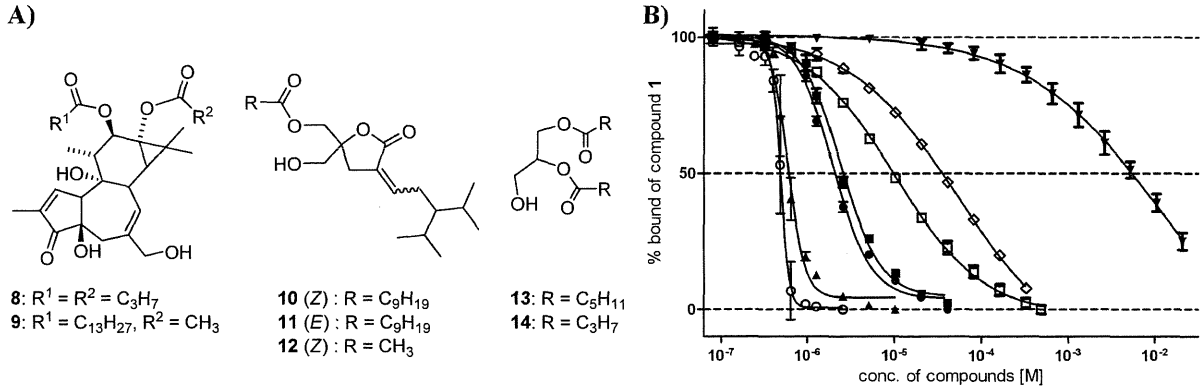

Figure 5. Competitive assay against compound **1** based on fluorescent intensity (spectrofluorometer). (A) Structures of test compounds. (B) Inhibition curves indicate results of compounds **8** (▲), **9** (○), **10** (●), **11** (■), **12** (□), **13** (◇), and **14** (▼).

Determination of K_i of Compounds for Full Length PKCδ. Enzyme–ligand interaction was assessed in vitro as the ability of the ligand to displace bound [20-^{3}H]phorbol 12,13-dibutyrate ([^{3}H]PDBu) from recombinant human PKCδ in the presence of phosphatidylserine (PS) in an experimental procedure that was described previously.[28] In constant concentration analysis, the concentrations of compounds were fixed at 100 nM for known compounds and at 10 μM for library compounds. The other procedures were the same as those of the standard evaluation.

Fluorescent Titration of the δC1b Domain. An amount of 25 μL of a solution of PS in chloroform (10 mg/mL) was evaporated to dryness under nitrogen. Then 50 mM Tris·HCl buffer (pH 7.4) was added and the PS was sonicated with a Microtip for a total of 15 s. A stock solution of compound **1** was diluted with 50 mM Tris·HCl buffer (pH 7.4) containing 100 μg/mL PS to prepare a 0.2 μM solution. The recombinant δC1b domain was added to the 0.2 μM solution of compound **1**, and fluorescent spectra (λ_{ex} = 340 nm) were measured at 25 °C. The concentration of the recombinant δC1b domain started at 0.01 μM and increased to 1.28 μM by titration. The final concentrations of compounds **2** and **3** were 0.2 and 0.05 μM, respectively. Change of fluorescent intensity (ΔF) was calculated at the following wavelengths, which showed λ_{max} in each evaluation; compound **1**, 406 (F_0) and 394 (F_1) nm; compound **2**, 520 (F_0) and 480 (F_1) nm; compound **3**, 463 (F_0) and 461 (F_1) nm. Wavelengths recorded before and after the addition of the δC1b domain.

Fluorescent Titration of Candidate Ligands. Compound **1** was diluted with 50 mM Tris·HCl (pH 7.4) containing 100 μg/mL PS to obtain a solution with a 0.2 μM final concentration. The δC1b domain was added to the above solution of compound **1** to be 0.96 μM. A candidate ligand was added to the solution, and fluorescent spectra were recorded with a spectrofluorometer at 25 °C. Fluorescent titration curves (λ_{em} = 407 nm) were analyzed by nonlinear regression, and IC_{50} values were estimated by a nonlinear least-squares curve-fitting method using GraphPad Prism 5 (GraphPad Software, Inc., La Jolla, CA, U.S.). In the constant concentration analysis, the concentrations of known compounds were fixed at 100 nM and of library compounds at 10 μM. The other procedures were the same as those in the standard evaluation.

Fluorescence-Quenching Analysis for Library Screening Recorded by Microplate Reader. Fluorescence intensity was recorded on Wallac ARVO MX (PerkinElmer) using a 96-well black plate. Compound **1** was diluted with 50 mM Tris·HCl (pH 7.4) containing 100 μg/mL PS to obtain a solution with a 0.2 μM final concentration. The δC1b domain was added to the above solution of compound **1** to be 0.96 μM. A candidate ligand (10 μM) was added to the compound **1**–δC1b domain complex solution, and fluorescent intensities (λ_{ex} = 355 nm, λ_{em} = 405 nm) were measured at 25 °C.

RESULTS AND DISCUSSION

Synthesis and Fluorescent Properties of Compounds 1–3. Three representative solvatochromic fluorophores, involving 6-methoxynaphthalene,[29] 5-(dimethylamino)naphthalene-1-sulfonyl (dansyl),[6,30,31] and diethylaminocoumarin,[32–35] have

dx.doi.org/10.1021/bc100567k |*Bioconjugate Chem.* 2011, 22, 923–930

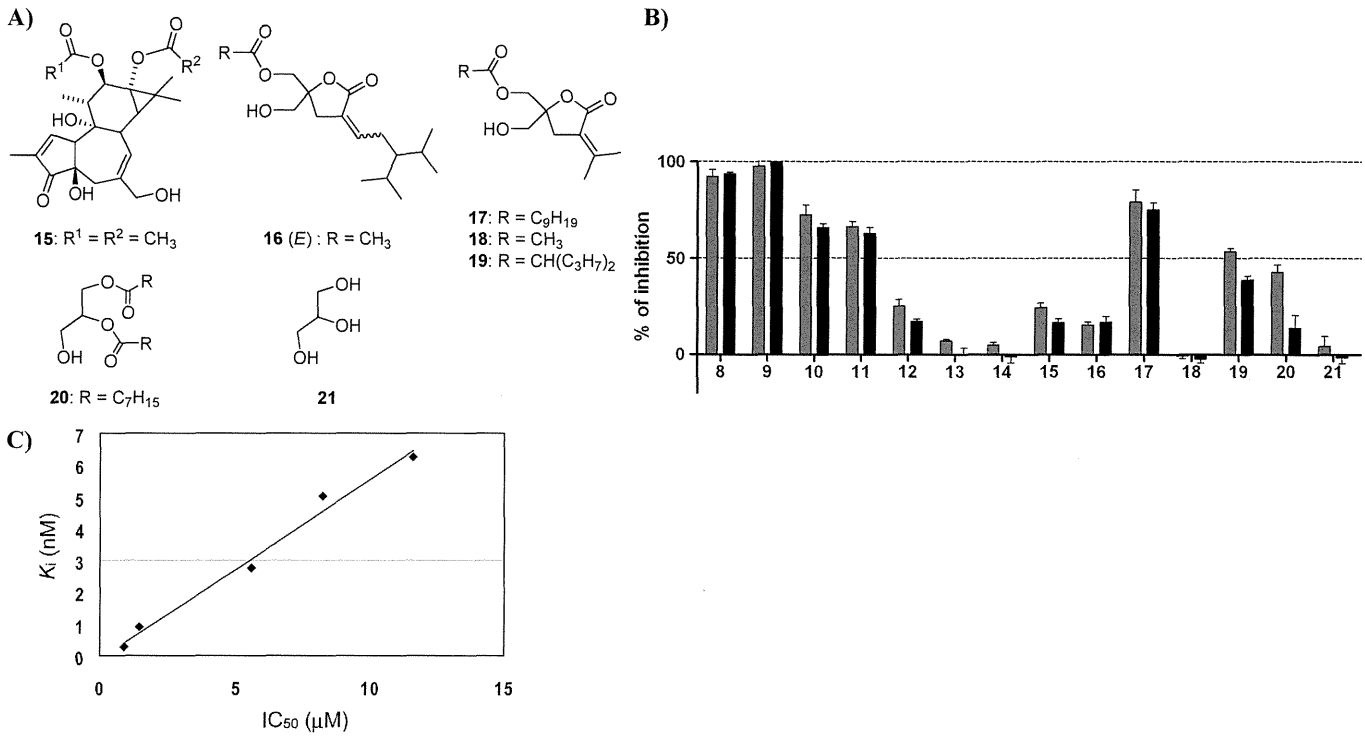

Figure 6. Comparison of inhibition percentages between the fluorescent assay (microplate reader) and the RI assay at a constant concentration of test compounds. (A) Structures of test compounds. (B) Inhibition of binding of compound **1** (fluorescent assay, left gray bars) or [^{3}H]PDBu (RI assay, right black bars) in the presence of test compounds (10 μM in the fluorescent assay and 100 nM in the RI assay). The final DMSO concentration is 4%. (C) Plots of IC_{50} values (μM) by the fluorescent assay versus K_i (nM) by the RI assay for compounds **8**, **9**, **10**, **11**, and **17**.

been utilized. The 6-methoxynaphthalene was incorporated at the α-carbon of the *sn*-1 carbonyl group of the DAG-lactone structure (Scheme 1). The dansyl and diethylaminocoumarin were incorporated into the *sn*-2 carbonyl group. In comparison with the fluorescent spectra of these compounds, obtained in various solvents, compound **1** showed the most variation with solvent polarity (Figure 2). It is known that solvatochromic fluorophores show higher fluorescent intensity in hydrophobic environments and that the fluorophores are sensitive to the environment of a binding pocket in target proteins. The fluorescent intensity of labeled DAG-lactones should reflect its binding to a target protein, PKCδ (Figure 3), and as expected, our reporter compounds **1** and **2** containing solvatochromic fluorophores exibited a remarkable increase of fluorescent intensity in the proximity of the C1b domain of PKCδ (δC1b), which is a specific target of DAG-lactone derivatives (Table 1 and Figure 4A). This indicates that in the binding of compounds **1** and **2** to the δC1b domain, the 6-methoxynaphthalene and dansyl moieties are located in the hydrophobic environment. However, for compound **3**, the fluorescent intensity was decreased as the concentration of δC1b increased. The spectra in various solvents showed dependence of the fluorescent intensity of the compound **3** on solvent polarity, and it was suggested that in the binding of compound **3** to the δC1b domain, the diethylaminocoumarin moiety could be located in the hydrophilic environment. The changes of fluorescent intensity of the synthetic compounds are summarized in Table 1. The binding constants of fluorescent compounds were evaluated by [^{3}H]PDBu competitive assay. Compound **1** showed the highest binding affinity for the δC1b domain. In the fluorescence-based analysis of binding, two factors are key to the sensitivity of the assay system: (i) the fluorescent change as a function of the ligand binding and (ii) the binding affinity of a reporter compound.

Evaluation of Binding to PKCδ by Fluorescent Change of Compound 1. The results obtained supported the selection of compound **1** as a reporter compound for further study. In competitive assays, when candidate ligands of PKCδ are present, they replace the fluorescent compounds, which are formerly bound to δC1b, and the fluorescent intensity should decrease. Practically, addition of PDBu to the complex of compound **1** and δC1b resulted in a remarkable decrease of fluorescent intensity (Figure 4B). By utilization of compound **1** as a reporter, binding analysis of known PKCδ ligands was performed to assess the reliability of the assay system. Compounds **8**−**14** were prepared as test compounds (Figure 5A), and their IC_{50} values, determined by the fluorescence-based competitive assay with a fluorospectrophotometer against compound **1**, were 0.60, 0.49, 1.95, 2.42, 10.0, 54.2, and 1.22 × 10^4 μM, respectively (Figure 5B). The order of the IC_{50} values of compounds **8**−**11** is identical to that of the K_i values (0.91, 0.26, 5.0, and 6.2 nM, respectively) determined by the [^{3}H]PDBu competitive assay.

The Binding Analysis by Competition with Compound 1 Showed Linearity with the Classical RI Assay. To further assess the collinearity of the fluorescent assay on microplates and the [^{3}H]PDBu assay, the inhibition percentages by compounds **8**−**21** in both assays (Figure 6A) at constant concentration were compared. The compound concentrations were set at 10 μM for the fluorescent assay and at 100 nM for the [^{3}H]PDBu assay. As shown in Figure 6B, the inhibition percentages of compounds **8**−**21** are similar in both assays. Comparison of the IC_{50} and K_i of compounds **8**, **9**, **10**, **11**, and **17**, possessing more than 60% inhibition percentages, showed acceptable linearity (Figure 6C).

dx.doi.org/10.1021/bc100567k |*Bioconjugate Chem.* 2011, 22, 923–930

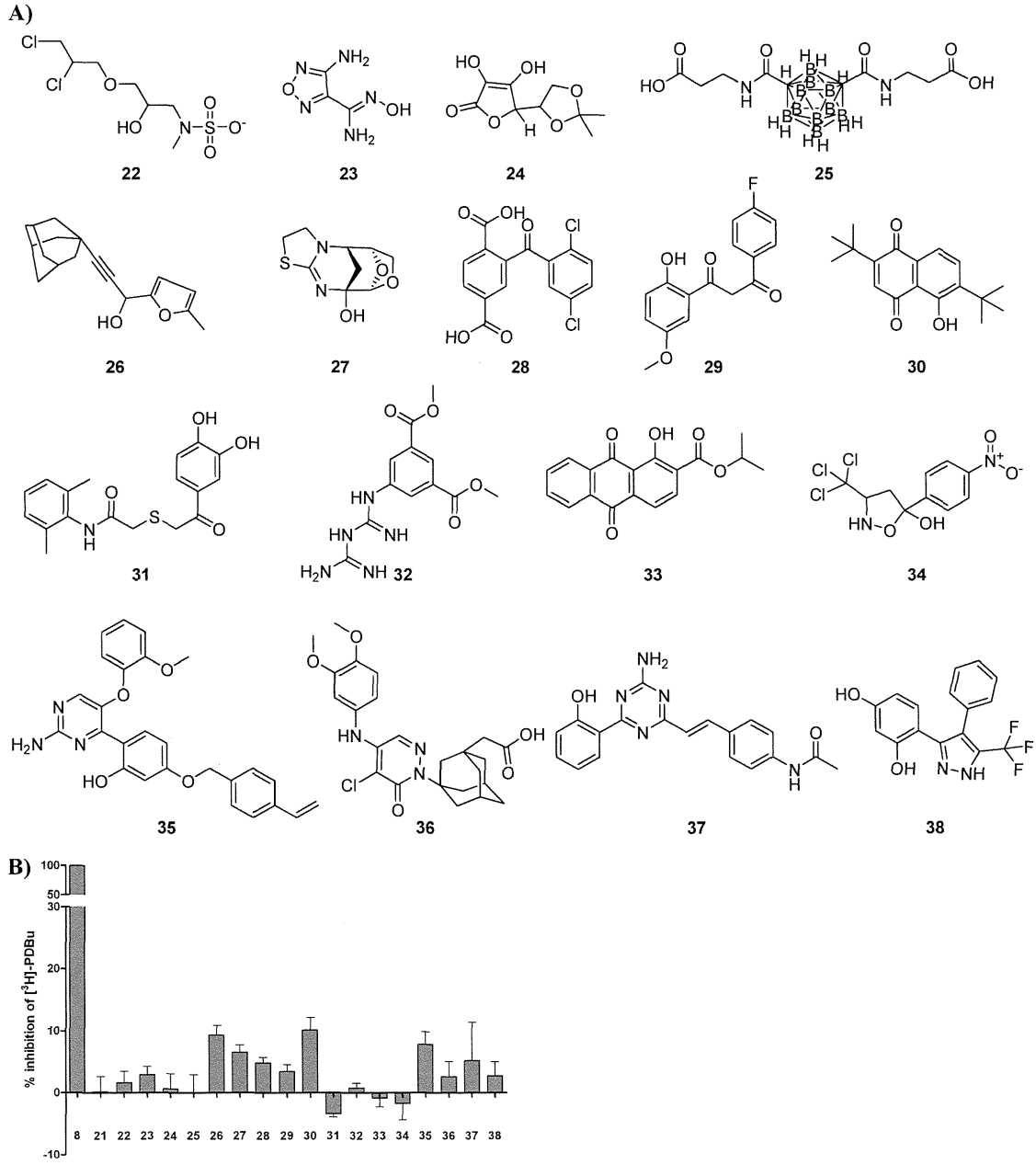

Figure 7. The RI competition assay of positive hit compounds found in fluorescent screening utilizing compound **1**. (A) Structures of test compounds obtained from screening. (B) Results of the inhibition assay based on RI methods. The concentration of compounds was fixed at 10 μM. The *X* axis indicates compound numbers. Columns show average inhibition obtained from triplicated experiments. Bars indicate standard errors.

In view of the above results, the present fluorescence-based evaluation of binding to the δC1b domain on microplates was deemed to be a promising alternative for the classical RI assay.

Expansion of the Fluorescence Evaluation to Screening of Library Compounds. As a proof-of-concept study, compound **1** was utilized in screening of a chemical library, supplied by the Screening Center at the Tokyo Medical and Dental University Screening Center. The structures of the library compounds were analyzed in advance of screening. For binding to the δC1b domain, pharmacophores including the carbonyl and hydroxy groups are necessary and only compounds including these functional groups were chosen. In the analysis of the library on microplates, compounds with more than 20% decrease of fluorescent intensity determined by triplicated assays were selected as candidates for further study. Compounds **22**−**38** were found from 2560 library compounds (Figure 7A) as candidate δC1b ligands. To further assess the binding affinity of these compounds, evaluation of binding by competition with the [^{3}H]PDBu was performed at a fixed concentration (10 μM) (Figure 7B). In this analysis, compounds **30** and **26**, with inhibition percentages at 10 μM of 10.2% and of 9.4%, respectively, showed the most and the second most potent binding affinities for the δC1b domain. The binding affinities of these compounds are still very low compared to that of DAG-lactones, but an SAR study of these compounds could lead to novel structure templates for synthetic PKC ligands. This analysis also revealed that compounds **24**, **25**, **31**, **32**, **33**, and **34** are false positive hits. The results obtained indicate that our screening system with a fluorescent

dx.doi.org/10.1021/bc100567k |*Bioconjugate Chem.* 2011, 22, 923–930

DAG-lactone derivative could be utilized for discovery of novel chemical leads for PKCδ.

CONCLUSION

A fluorescence-based method for chemical library screening has been developed. This method, which requires no washing steps, provides a linear response in relative binding affinity between compounds and is compatible with the classical RI assay for PKC ligands. By screening of more than 2500 library compounds, the method was proven to be a reliable means of discovery of compounds that bind to the C1b domain of PKCδ. The method would provide potent lead compounds that bind to the isozyme utilized in the assay. By utilization of the difference of the binding affinity of reporter compounds to different isozymes, it is possible that this screening system can provide an efficient selection of lead compounds highly specific to a target isozyme. This fluorescence-quenching method should be applicable to other known receptor−ligand combinations.

ASSOCIATED CONTENT

Supporting Information. Synthesis procedures and NMR, HRMS, and IR data. This material is available free of charge via the Internet at http://pubs.acs.org.

AUTHOR INFORMATION

Corresponding Author

*E-mail: tamamura.mr@tmd.ac.jp. Phone: +81-3-5280-8036. Fax: +81-3-5280-8039.

ACKNOWLEDGMENT

The authors thank Professor Masatoshi Hagiwara and Dr. Yukiko Okuno (Chemical Biology Screening Center, Tokyo Medical and Dental University) for their support in chemical library screening. This work was supported in part by Naito Foundation (W.N.) and Research Award of Graduate School of Biomedical Science, Tokyo Medical and Dental University (W.N. and T.I.)

REFERENCES

(1) Loving, G. S., Sainlos, M., and Imperiali, B. (2010) Monitoring protein interactions and dynamics with solvatochromic fluorophores. *Trends Biotechnol. 28*, 73–83.

(2) Rothman, D. M., Shults, M. D., and Imperiali, B. (2005) Chemical approaches for investigating phosphorylation in signal transduction networks. *Trends Cell Biol. 15*, 502–510.

(3) Terai, T., and Nagano, T. (2008) Fluorescent probes for bioimaging applications. *Curr. Opin. Chem. Biol. 12*, 515–521.

(4) Reymond, J. -L. (2008) Substrate arrays for fluorescence-based enzyme fingerprinting and high-throughput screening. *Ann. N.Y. Acad. Sci. 1130*, 12–20.

(5) Nomura, W., Tanabe, Y., Tsutsumi, H., Tanaka, T., Ohba, K., Yamamoto, N., and Tamamura, H. (2008) Fluorophore labeling enables imaging and evaluation of specific CXCR4−ligand interaction at the cell membrane for fluorescence-based screening. *Bioconjugate Chem. 19*, 1917–1920.

(6) Hayashida, O., Ogawa, N., and Uchiyama, M. (2007) Surface recognition and fluorescence sensing of histone by dansyl-appended cyclophane-based resorcinarene trimer. *J. Am. Chem. Soc. 129*, 13698–13705.

(7) Tsutsumi, H., Nomura, W., Abe, S., Mino, T., Masuda, A., Ohashi, N., Tanaka, T., Ohba, K., Yamamoto, N., Akiyoshi, K., and Tamamura, H. (2009) Fluorogenically active leucine zipper peptides as tag-probe pairs for protein imaging in living cells. *Angew. Chem., Int. Ed. 48*, 9164–9166.

(8) Nishizuka, Y. (1992) Intracellular signaling by hydrolysis of phospholipids and activation of protein kinase C. *Sceince 258*, 607–614.

(9) Newton, A. C. (1995) Protein kinase C: structure, function, and regulation. *J. Biol. Chem. 270*, 28495–28498.

(10) Watanabe, T., Ono, Y., Taniyama, Y., Hazama, K., Igarashi, K., Ogita, K., Kikkawa, U., and Nishizuka, Y. (1992) Cell division arrest induced by phorbol ester in CHO cells overexpressing protein kinase C-delta subspecies. *Proc. Natl. Acad. Sci. U.S.A. 89*, 10159–10163.

(11) Mischak, H., Pierce, J. H., Goodnight, J., Kazanietz, M. G., Blumberg, P. M., and Mushinski, J. F. (1993) Phorbol ester-induced myeloid differentiation is mediated by protein kinase C-alpha and -delta and not by protein kinase C-beta II, -epsilon, -zeta, and -eta. *J. Biol. Chem. 268*, 20110–20115.

(12) Li, C., Wernig, F., Leitges, M., Hu, Y., and Xu, Q. (2003) Mechanical stress-activated PKCdelta regulates smooth muscle cell migration. *FASEB J. 17*, 2106–2108.

(13) Ghayur, T., Hugunin, M., Talanian, R. V., Ratnofsky, S., Quinlan, C., Emoto, Y., Pandey, P., Datta, R., Huang, Y., Kharbanda, S., Allen, H., Kamen, R., Wong, W., and Kufe, D. (1996) Proteolytic activation of protein kinase C delta by an ICE/CED 3-like protease induces characteristics of apoptosis. *J. Exp. Med. 184*, 2399–2404.

(14) Alkon, D. L., Sun, M.-K., and Nelson, T. J. (2007) PKC signaling deficits: a mechanistic hypothesis for the origins of Alzheimer's disease. *Trends Pharmacol. Sci. 28*, 51–60.

(15) Wang, Q. J. (2006) PKD at the crossroads of DAG and PKC signaling. *Trends Pharmacol. Sci. 27*, 317–323.

(16) Marquez, V. E., and Blumberg, P. M. (2003) Synthetic diacylglycerols (DAG) and DAG-lactones as activators of protein kinase C (PK-C). *Acc. Chem. Res. 36*, 434–443.

(17) Nacro, K., Bienfait, B., Lee, J., Han, K.-C., Kang, J.-H., Benzaria, S., Lewin, N. E., Bhattacharyya, D. K., Blumberg, P. M., and Marquez, V. E. (2000) Conformationally constrained analogues of diacylglycerol (DAG). 16. How much structural complexity is necessary for recognition and high binding affinity to protein kinase C?. *J. Med. Chem. 43*, 921–944.

(18) Tamamura, H., Bienfait, B., Nacro, K., Lewin, N. E., Blumberg, P. M., and Marquez, V. E. (2000) Conformationally constrained analogues of diacylglycerol (DAG). 17. Contrast between *sn*-1 and *sn*-2 DAG lactones in binding to protein kinase C. *J. Med. Chem. 43*, 3209–3217.

(19) Tamamura, H., Sigano, D. M., Lewin, N. E., Blumberg, P. M., and Marquez, V. E. (2004) Conformationally constrained analogues of diacylglycerol. 20. The search for an elusive binding site on protein kinase C through relocation of the carbonyl pharmacophore along the *sn*-1 side chain of 1,2-diacylglycerol lactones. *J. Med. Chem. 47*, 644–655.

(20) Baba, Y., Ogoshi, Y., Hirai, G., Yanagisawa, T., Nagamatsu, K., Mayumi, S., Hashimoto, Y., and Sodeoka, M. (2004) Design, synthesis, and structure−activity relationship of new isobenzofuranone ligands of protein kinase C. *Bioorg. Med. Chem. Lett. 14*, 2963–2967.

(21) Baba, Y., Mayumi, S., Hirai, G., Kawasaki, H., Ogoshi, Y., Yanagisawa, T., Hashimoto, Y., and Sodeoka, M. (2004) Evaluation of series of isobenzofuranone dimers as PKCalpha ligands: implication for the distance between the two ligand binding sites. *Bioorg. Med. Chem. Lett. 14*, 2969–2972.

(22) Yanagita, R. C., Nakagawa, Y., Yamanaka, N., Kashiwagi, K., Saito, N., and Irie, K. (2008) Synthesis, conformational analysis, and biological evaluation of 1-hexylindolactam-V10 as a selective activator for novel protein kinase C isozymes. *J. Med. Chem. 51*, 46–56.

(23) Nakagawa, Y., Yanagita, R. C., Hamada, N., Murakami, A., Takahashi, H., Saito, N., Nagai, H., and Irie, K. (2009) A simple analogue of tumor-promoting aplysiatoxin is an antineoplastic agent rather than a tumor promoter: development of a synthetically accessible protein kinase C activator with bryostatin-like activity. *J. Am. Chem. Soc. 131*, 7573–7579.

(24) Martin, S. F., Josey, J. A., Wong, Y.-L., and Dean, D. W. (1994) General method for the synthesis of phospholipid derivatives of 1,2-*O*-diacyl-*sn*-glycerols. *J. Org. Chem. 59*, 4805–4820.

(25) Malolanarasimhan, K., Kedei, N., Sigano, D. M., Kelley, J. A., Lai, C. C., Lewin, N. E., Surawski, R. J., Pavlyukovets, V. A., Garfield, S. H., Wincovitch, S., Blumberg, P. M., and Marquez, V. E. (2007) Conformationally constrained analogues of diacylglycerol (DAG). 27. Modulation of membrane translocation of protein kinase C (PKC) isozymes alpha and delta by diacylglycerol lactones (DAG-lactones) containing rigid-rod acyl groups. *J. Med. Chem. 50*, 962–978.

(26) Nomura, W., Narumi, T., Ohashi, N., Serizawa, Y., Lewin, N. E., Blumberg, P. M., Furuta, T., and Tamamura, H. (2011) Synthetic caged DAG-lactones for photochemically-controlled activation of protein kinase C. *ChemBioChem 12*, 535–539.

(27) Mischak, H., Bodenteich, A., Kolch, W., Goodnight, J., Hofer, F., and Mushinski, J. F. (1991) Mouse protein kinase C-delta, the major isoform expressed in mouse hemopoietic cells: sequence of the cDNA, expression patterns, and characterization of the protein. *Biochemistry 30*, 7925–7931.

(28) Kazanietz, M. G., Krausz, K. W., and Blumberg, P. M. (1992) Differential irreversible insertion of protein kinase C into phospholipid vesicles by phorbol esters and related activators. *J. Biol. Chem. 267*, 20878–20886.

(29) List, B., Barbas, C. F., III, and Lerner, R. A. (1998) Aldol sensors for the rapid generation of tunable fluorescence by antibody catalysis. *Proc. Natl. Acad. Sci. U.S.A. 95*, 15351–15355.

(30) Davis, G. A. (1972) Dansylglycine as a fluorescent probe for aqueous solutions of cationic detergents. *J. Am. Chem. Soc. 94*, 5089–5090.

(31) Morii, T., Sugimoto, K., Makino, K., Otsuka, M., Imoto, K., and Mori, Y. (2002) A new fluorescent biosensor for inositol trisphosphate. *J. Am. Chem. Soc. 124*, 1138–1139.

(32) Matlock, D. L., and Heyduk, T. (1999) A real-time fluorescence method to monitor the melting of duplex DNA during transcription initiation by RNA polymerase. *Anal. Biochem. 270*, 140–147.

(33) Kakio, A., Nishimoto, S., Yanagisawa, K., Kozutsumi, Y., and Matsuzaki, K. (2001) Cholesterol-dependent formation of GM1 ganglioside-bound amyloid beta-protein, an endogenous seed for Alzheimer amyloid. *J. Biol. Chem. 276*, 24985–24990.

(34) Timofeevski, S. L., Prusakiewicz, J. J., Rouzer, C. A., and Marnett, L. J. (2002) Isoform-selective interaction of cyclooxygenase-2 with indomethacin amides studied by real-time fluorescence, inhibition kinetics, and site-directed mutagenesis. *Biochemistry 41*, 9654–9662.

(35) Sakamoto, S., and Kudo, K. (2008) Supramolecular control of split-GFP reassembly by conjugation of beta-cyclodextrin and coumarin units. *J. Am. Chem. Soc. 130*, 9574–9582.

(36) Sharkey, N. A., and Blumberg, P. M. (1985) Highly lipophilic phorbol esters as inhibitors of specific [^{3}H]phorbol 12,13-dibutyrate binding. *Cancer Res. 45*, 19–24.

(37) Ohashi, N., Nomura, W., Kato, M., Narumi, T., Lewin, N. E., Blumberg, P. M., and Tamamura, H. (2009) Synthesis of protein kinase Cdelta C1b domain by native chemical ligation methodology and characterization of its folding and ligand binding. *J. Pept. Sci. 15*, 642–646.

JACS
JOURNAL OF THE AMERICAN CHEMICAL SOCIETY
ARTICLE
pubs.acs.org/JACS

Boron Cluster-based Development of Potent Nonsecosteroidal Vitamin D Receptor Ligands: Direct Observation of Hydrophobic Interaction between Protein Surface and Carborane

Shinya Fujii,[†,‡] Hiroyuki Masuno,[‡] Yoshiyuki Taoda,[§] Atsushi Kano,[†,‡] Angsuma Wongmayura,[⊥] Makoto Nakabayashi,[†] Nobutoshi Ito,[†] Masato Shimizu,[†,‡] Emiko Kawachi,[†,‡] Tomoya Hirano,[‡] Yasuyuki Endo,[∥] Aya Tanatani,[⊥] and Hiroyuki Kagechika*[,†,‡]

[†]Graduate School of Biomedical Science and [‡]Institute of Biomaterials and Bioengineering, Tokyo Medical and Dental University, 2-3-10, Kanda-Surugadai, Chiyoda-ku, Tokyo 101-0062, Japan

[§]Graduate School of Pharmaceutical Sciences, University of Tokyo, 7-3-1, Hongo, Bunkyo-ku, Tokyo 113-0033, Japan

[⊥]Department of Chemistry, Faculty of Science, Ochanomizu University, 2-1-1 Otsuka, Bunkyo-ku, Tokyo 112-8610, Japan

[∥]Faculty of Pharmaceutical Sciences, Tohoku Pharmaceutical University, 4-4-1 Komatsushima, Aoba-ku, Sendai 981-8558, Japan

Supporting Information

ABSTRACT: We report here the design and synthesis of a novel vitamin D receptor (VDR) agonist whose hydrophobic core structure is *p*-carborane (1,12-dicarba-*closo*-dodecaborane, an icosahedral carbon-containing boron cluster having remarkable thermal and chemical stability and a characteristically hydrophobic B−H surface). This carborane-based VDR ligand exhibited moderate vitamin D activity, comparable to that of the natural hormone, despite its simple and flexible structure. X-ray structure analysis provided direct evidence that the carborane cage binds to the hydrophobic surface of the ligand-binding pocket of the receptor, promoting transition to the active conformation. These results indicate that the spherical B−H surface of carborane can function efficiently as a hydrophobic anchor in binding to the receptor surface, thereby allowing induced fitting of the three essential hydroxyl groups on the alkyl chains to the appropriate positions for interaction with the VDR binding site, despite the entropic disadvantage of the flexible structure. We suggest that carborane structure is a promising option in the design of novel drug candidates.

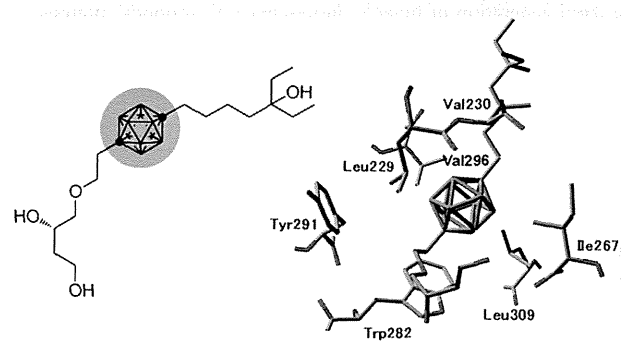

INTRODUCTION

Icosahedral carboranes (dicarba-*closo*-dodecaboranes; Figure 1), which are polyhedral carbon-containing boron clusters, have a bulky spherical structure and exhibit high hydrophobicity as well as having high thermal and chemical stability.[1] The remarkable stability of carboranes makes their derivatives particularly suitable for specialized applications, e.g., in polymers for high-temperature use and as neutron-shielding materials. In the field of life sciences, carboranes are considered to be candidates for boron neutron capture therapy (BNCT) of cancer, based on the nuclear reaction between ^{10}B nuclei and thermal neutrons.[2] Various types of compounds have been prepared, including amino acid derivatives, nucleic acid derivatives, and porphyrin derivatives, with the aim of incorporating ^{10}B atoms selectively into cancer cells,[3] but the carborane cage has been regarded as simply a boron carrier. Little attention has been paid to the possibility of using the spherical hydrophobic B−H surface, the most characteristic feature of carboranes, to obtain biologically active molecules.[4] Hydrophobic interaction plays an essential role in interactions between proteins and bioactive compounds, and therefore the use of carboranes as a hydrophobic core could make it possible to develop a novel class of biologically active molecules. In particular, hydrophobic structure is important for nuclear receptor ligands, such as steroid hormones and activated vitamins, to bind effectively to their specific receptors.[5] We have applied the carborane cage as a hydrophobic structural moiety of nuclear receptor ligands and developed novel carborane-based ligands for nuclear receptors, such as androgen receptor (AR),[6] estrogen receptor (ER),[7] and retinoid receptors.[8]

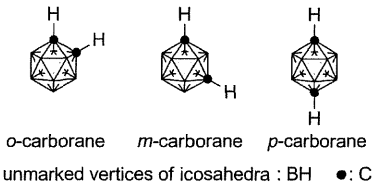

Figure 1. Structures of carboranes.

Received: September 19, 2011
Published: November 08, 2011

 © 2011 American Chemical Society

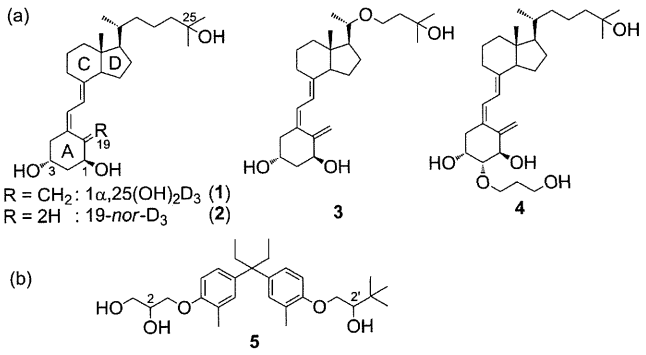

Figure 2. Structures of (a) vitamin D derivatives with secosteroid structure and (b) a nonsecosteroidal VDR ligand.

These carborane-based nuclear receptor ligands bearing an unnatural hydrophobic core structure, i.e., nonsteroidal and nonterpenoidal ligands, are advantageous for separation of pleiotropic receptor functions as well as having excellent chemical stability.

Vitamin D receptor (VDR) is the ligand-inducible nuclear receptor for vitamin D and plays important roles in many physiological processes, including calcium and phosphate homeostasis, bone metabolism, immune regulation, cell proliferation, and differentiation.[9] VDR is activated by binding of the endogenous agonist, 1α,25-dihydroxyvitamin D_3 [1α,25(OH)$_2$D$_3$; **1**], a metabolically activated form of vitamin D_3, and regulates expression of specific target genes. VDR and its ligands have significant roles in the pathogenesis and therapy of diseases, such as osteoporosis, arthritis, psoriasis, and cancers. Thus, thousands of VDR ligands have been synthesized and biologically evaluated as drug candidates, leading to the clinical application of maxacalcitol (**3**) and eldecalcitol (**4**).[10]

Structurally, almost all of the developed VDR ligands with high potency have the same secosteroidal skeleton as **1** or **2**, consisting of the A-ring bearing two hydroxyl groups, a conjugated diene or triene moiety, the CD-ring, and a side chain (Figure 2). Although secosteroidal derivatives have high potency, their structural complexity, synthetic inconvenience, and chemical instability are disadvantageous for potential clinical application. Further, there are strict structural requirements, such as the substituent configuration on the A ring in the secosteroid structure. Though some work has been done to develop nonsecosteroidal VDR ligands, such as des-C and/or D ring derivatives of **1**[11] and bisphenol derivatives such as **5**,[12] in the past decade, it remains important to discover potent nonsecosteroidal VDR ligands. Nonsecosteroidal compounds would be useful as clinical drug candidates and as tools for investigation of VDR function, by analogy with nonsteroidal ligands of steroid hormone receptors, such as the ER ligands tamoxifen and raloxifene[13] and the AR ligands flutamide and bicalutamide. Herein, we describe the development of nonsecosteroidal VDR ligands, based on the carborane cage, and we also report the direct observation, by means of X-ray crystal structure analysis, of the interaction between a carborane-based VDR ligand and the specific receptor.[14]

■ RESULTS

Design and Synthesis of Carborane-Based VDR Ligand Candidates. Four structural elements are required for effective binding to VDR: one is a hydrophobic core with appropriate

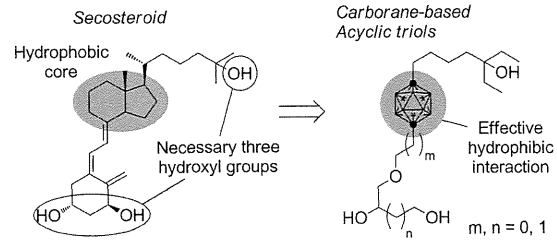

Figure 3. Design strategy for novel nonsecosteroidal VDR ligands bearing a carborane cage.

bulkiness, that corresponds to the CD-ring of **1**, and the others are three appropriately positioned hydroxyl groups. We assumed that the CD-ring of secosteroidal structure could be replaced by a carborane cage, from the viewpoints of spatial size, hydrophobicity, and stability. Regarding hydrophilic moieties, structure–activity relationship studies on secosteroidal vitamin D analogs have revealed that the configuration and conformation of hydroxyl groups, especially the hydroxyl groups at the 1- and 3-positions of the A-ring, are critical for vitamin D potency. We assumed, however, that a flexible dihydroxyalkyl group would be able to function as an alternative to the dihydroxylated A-ring, if the hydrophobic carborane cage functions as potent anchor in binding. Generally, a flexible backbone is entropically less effective than cyclic structure to retain active conformation. However, if the carborane cage interacts strongly with the hydrophobic surface of the receptor, the flexible alkyl chains might permit induced fitting of the three hydroxyl groups to the positions required for VDR binding, so that the whole molecule would function as a VDR ligand. A few opened A-ring analogs of **1** were synthesized, and application of the flexible diol as the hydrophilic pharmacophore of VDR ligands had been suggested.[15] Further, the lack of conjugated diene or triene structure would make the compound more stable chemically. On the basis of the above considerations, we designed a series of dialkylcarborane derivatives which have three hydroxyl groups bound to flexible acyclic alkyl or ether chains (Figure 3).

As a hydrophobic core, we chose *p*-carborane, considering the geometry of the carbon atoms, at which substituents are introduced and the fact that it has the highest hydrophobicity among the three stereoisomers of carborane.[16] Diethylcarbinol was selected as the side chain terminal in place of the dimethylcarbinol of **1** based on previous reports that indicated diehylcarbinol moiety enhanced the vitamin D potency.[17] An ether oxygen atom was introduced into the dihydroxyalkyl chain to provide efficient synthetic approaches. In addition, the less hindered oxa tethering chain may be favorable for avoiding steric repulsion between the chain and the hydrophobic carborane core.[18]

The designed carborane derivatives were synthesized from *p*-carborane (Scheme 1). The hydrogen atom on carbon of the carborane cage is sufficiently acidic to be removed by a strong base, such as butyl lithium, and the resulting C-lithiated form of carborane is a good nucleophilic reagent.[19] Thus, a 2-benzyloxyethyl group was introduced at the carbon atoms of *p*-carborane with *n*-butyl lithium and benzyl 2-bromoethyl ether to afford **6**. Introduction of a 5-ethyl-5-triethylsilyloxyheptyl group, corresponding to the side chain of **1**, gave **7**, and subsequent removal of the benzyl group gave the common intermediate **8**. Ether formation of **8** with appropriate tosylates gave the corresponding triol precursor **9** or **11**. Deprotection of three hydroxyl groups under acidic conditions afforded the target compounds **10** and **12**.

Scheme 1. Synthetic Scheme of Designed Carborane Derivatives[a]

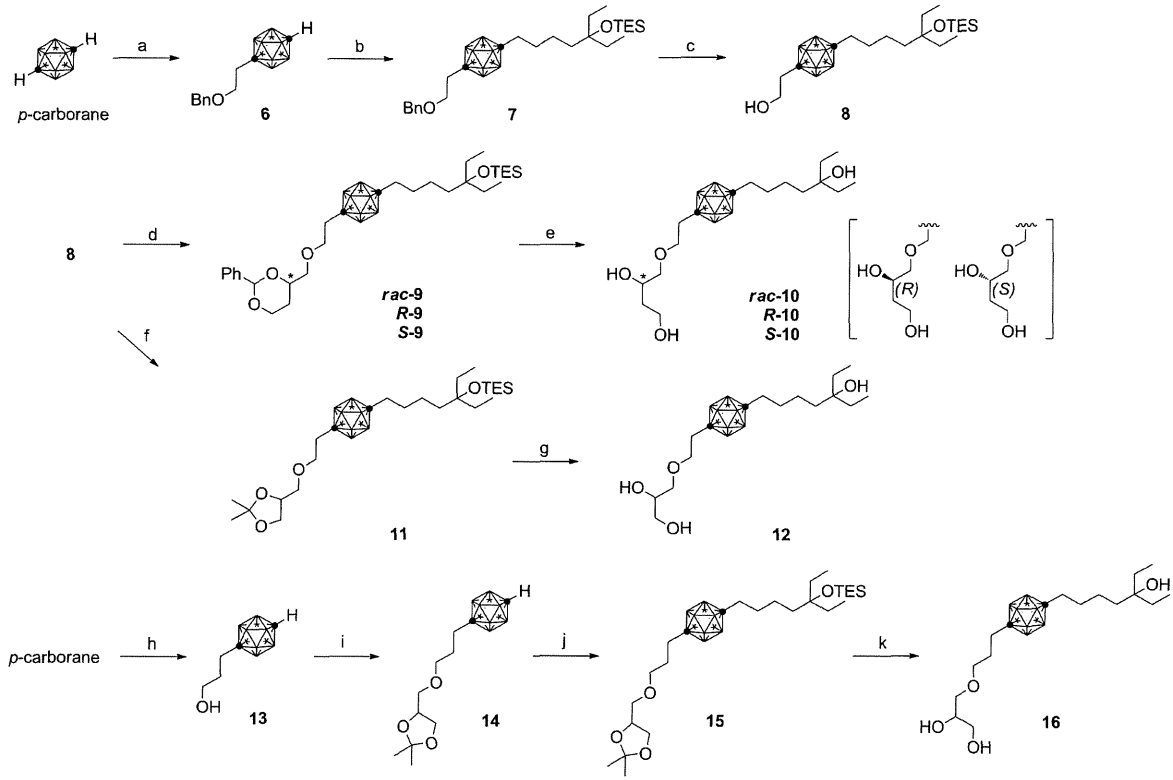

[a] Conditions: (a) *n*-BuLi, benzyl 2-bromoethyl ether, THF, 44%; (b) *n*-BuLi, 7-bromo-3-ethyl-3-triethylsilyloxyheptane, THF, ether, 96%; (c) H_2, Pd/C, EtOH-THF, 91%; (d) NaH, 4-(*p*-toluenesulfonyloxymethyl)-2-phenyl-1,3-dioxane, DMF, 17%; (e) HCl, MeOH-THF-H_2O, 96%; (f) NaH, 4-(*p*-toluenesulfonyloxymethyl)-2,2-dimethyl-1,3-dioxolane, DMF, 45%; (g) HCl, MeOH-THF-H_2O, 92%; (h) *n*-BuLi, trimethylene oxide, ether, 36%; (i) NaH, 4-(*p*-toluenesulfonyloxymethyl)-2,2-dimethyl-1,3-dioxolane, DMF, 26%; (j) *n*-BuLi, 7-bromo-3-ethyl-3-triethylsilyloxyheptane, THF, 94%; and (k) HCl, MeOH-THF-H_2O, 71%. Bn = benzyl, DMF = *N*,*N*-dimethylformamide, TES = triethylsilyl, and THF = tetrahydrofuran.

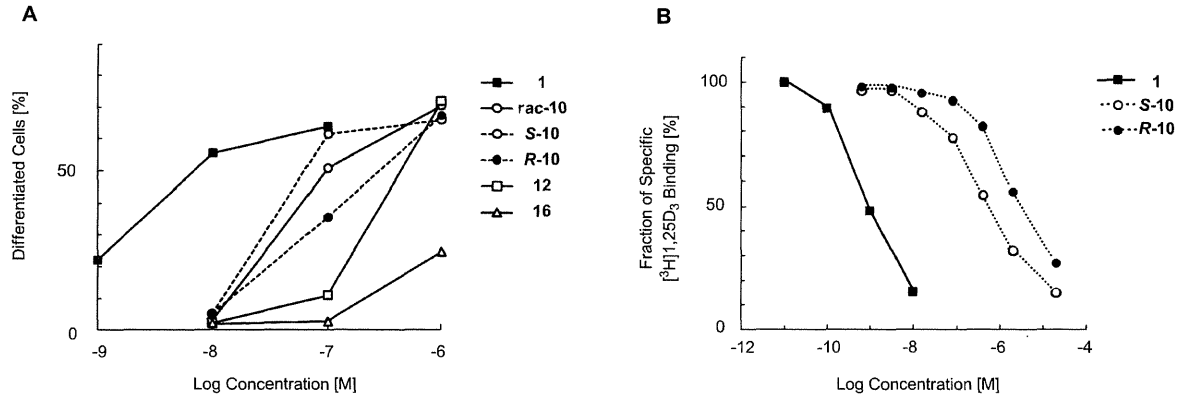

Figure 4. Biological evaluation of carborane derivatives. (A) HL-60 cell differentiation-inducing potency of carborane compounds in the concentration range of 10^{-9} to 10^{-6} M. Cell differentiation was determined as the ratio of NBT-positive cells. (B) Competitive binding assay of carborane derivatives using bovine thymus VDR-LBD and [^{3}H]1α,25(OH)$_2$D$_3$.

Two stereoisomers of **10** were also synthesized by use of the corresponding chiral tosylates.

Compound **16** bearing the other diol structure was also prepared from *p*-carborane in four steps. The lithiated form of *p*-carborane reacted with trimethylene oxide to afford 3-hydroxypropylcarborane **13**, and then ether formation gave **14**. The side chain moiety was introduced into **14** to afford **15**, and removal of protective groups under acidic conditions gave the triol **16**.

HL-60 Cell Differentiation-Inducing Activity. Vitamin D activity of the synthesized molecules **10**, **12**, and **16** was evaluated in terms of cell differentiation-inducing activity toward human acute promyelocytic leukemia cell line HL-60.[20] These carborane derivatives induced HL-60 cell differentiation in a dose-dependent manner (Figure 4A), and racemic **10** exhibited substantial activity; its potency was approximately one-twentieth of that of **1** and nearly equal to the reported potency of 19-*nor*-D$_3$ (**2**).[9,15]

dx.doi.org/10.1021/ja208797n |*J. Am. Chem. Soc.* 2011, 133, 20933–20941

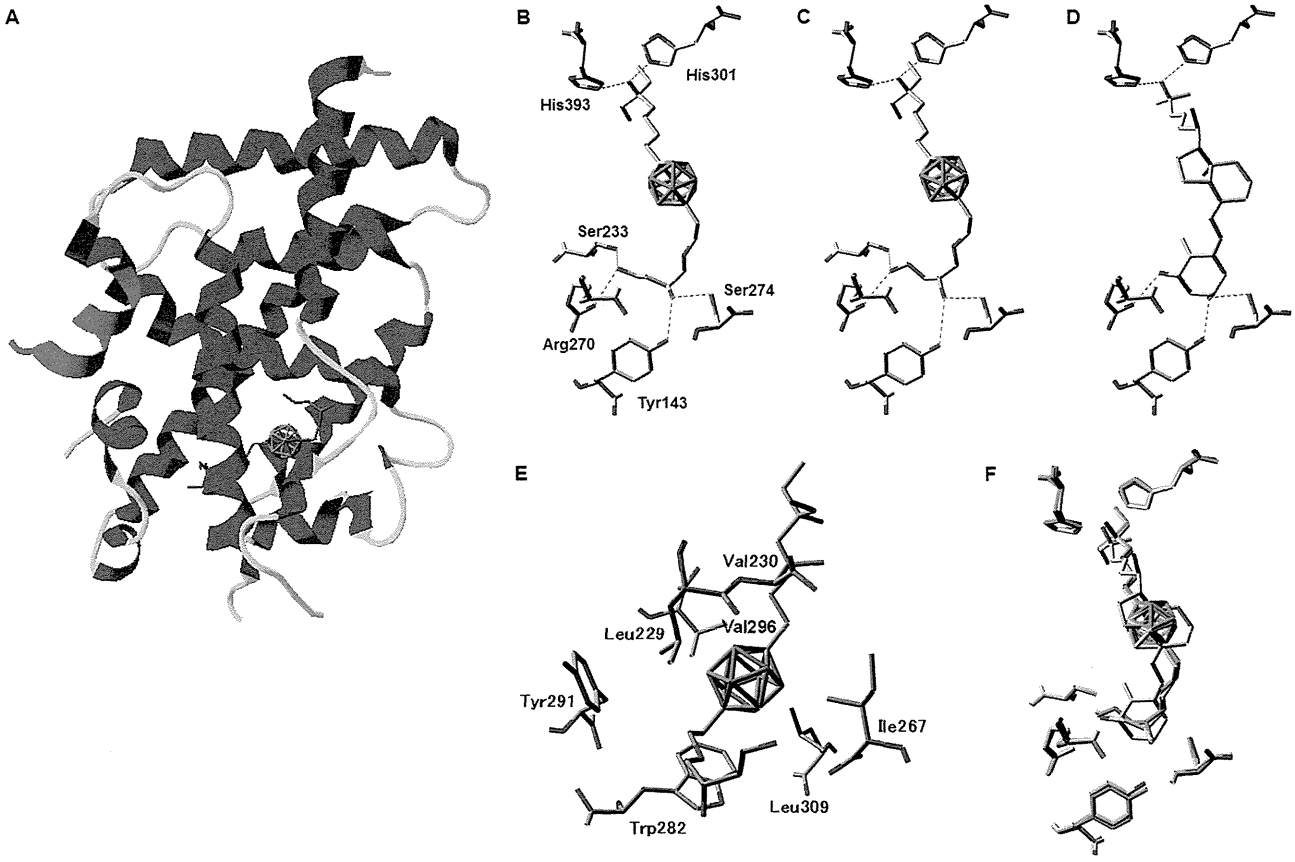

Figure 5. Structures of ligand-bound rat VDR-LBD and coactivator peptide (derived from DRIP205) complexes. (A) Structure of rat VDR-LBD bound to (*S*)-**10**. The coactivator peptide is shown in magenta. (B) Binding mode of (*S*)-**10** to VDR. (C) Binding mode of (*R*)-**10** to VDR. (D) Binding mode of **1** to VDR (PDB ID; 1RK3, ref 21). (E) Hydrophobic residues near the carborane cage of (*S*)-**10**. (F) Superimposition of ligand-binding pockets of the rat VDR-LBD complexed with the ligands: orange for complex of (*S*)-**10**, green for (*R*)-**10** and gray for 1α,25(OH)$_2$D$_3$ (**1**).

Therefore we prepared two enantiomers of **10** and investigated the vitamin D activities. Among the two enantiomers, the *S*-isomer ((*S*)-**10**) exhibited higher potency than the *R*-isomer ((*R*)-**10**). Therefore, *S*-configuration of the hydroxyl group is preferred for vitamin D activity, though the difference of potency between the two isomers was not very large. Compound **12**, bearing 1,2-diol structure, exhibited moderate activity, being less potent than compound **10**. Compound **16** exhibited quite low potency.

VDR-Binding Affinity of Carborane Derivatives. The binding affinity of selected compounds was examined by competitive binding assay using [^{3}H]1α,25(OH)$_2$D$_3$ and bovine thymus VDR ligand-binding domain (LBD) to determine whether the carborane derivatives bind directly to VDR. Figure 4B shows the dose–response curves of receptor binding of the carborane derivatives. Compounds (*S*)-**10** and (*R*)-**10** exhibited dose-dependent binding (IC_{50} = 0.64 and 4.1 μM, respectively). Although their binding potency was lower than that estimated from their functional potency toward HL-60 cells, low binding affinity of nonsecosteroidal VDR ligands was also reported in the case of bisphenol derivatives. Some physicochemical properties of these synthetic ligands may influence the potency, depending on the in vitro assay system. Nevertheless, the binding data were consistent with the results of HL-60 cell differentiation assay: the *S*-isomer of **10** exhibited higher potency than the *R*-isomer.

Structure of Complexes of Novel Carborane Derivatives with VDR. In order to understand the molecular basis of the interaction between the carborane hydrophobic core structure and the specific receptor protein, X-ray crystal structure analyses of VDR-LBD bound to (*S*)-**10** and (*R*)-**10** were conducted using the rat VDR-LBD, whose amino acid sequence in the ligand-binding pocket is identical to that of human VDR-LBD. The structure of rat VDR-LBD complexed with (*S*)-**10** in the presence of the coactivator peptide was determined at 1.93 Å resolution (PDB ID; 3VJS), and that of the complex of the less potent stereoisomer (*R*)-**10** at 2.0 Å resolution (PDB ID; 3VJT).

Figure 5A shows the structure of the complex of VDR-LBD and the most potent carborane derivative (*S*)-**10**. The overall structure of the VDR-LBD bound to (*S*)-**10** is essentially similar to that of VDR-LBD bound to **1** (PDB ID; 1RK3).[21] The coactivator peptide is bound to the AF-2 surface and is located at a typical position for agonist binding. This is a significant result, since the ligand-inducible activation of VDR depended on the three-dimensional structure of holo-VDR. VDR changes its conformation dramatically upon binding to the agonist. Depending on the nature of the induced three-dimensional structural change of VDR, a ligand may act as a partial agonist or antagonist. Carborane derivatives bearing flexible acyclic hydroxyalkyl chains can induce the active conformation of VDR, even though their structure is essentially different from that of secosteroid derivative **1**.

The acyclic triol (*S*)-**10** is located in the same pocket of the LBD as **1**. The structure of (*S*)-**10** in the ligand-binding pocket is shown in detail in Figure 5B. In the complex, the carborane

Table 1. Comparison of Hydrogen-Bond Distances between Ligand and Amino Acid Residues

	(*S*)-**10**, Å	(*R*)-**10**, Å	1α,25(OH)$_2$D$_3$ (**1**), Å
Ser 233 (Og)···O	2.79	2.70	2.75
Arg 270 (Nh)···O	2.94	2.88	2.83
Tyr 143 (Oh)···O	2.83	3.19	2.67
Ser 274 (Og)···O	2.96	3.24	2.94
His 301 (Ne) ···O	2.68	2.69	2.85
His 393 (Ne) ···O	2.94	3.01	2.70

moiety of (*S*)-**10** binds at the hydrophobic region of the VDR LBD, where the CD ring of **1** would be located (Figure 5E). The carborane is surrounded by hydrophobic amino acids residues (Leu229, Val230, Ile267, Trp282, Tyr291, Val296, and Leu309). The three hydroxyl groups of (*S*)-**10** form hydrogen bonds to residues of the receptor in a similar manner to that in the case of **1** (Figure 5B, D and Table 1). Thus, the terminal primary hydroxyl group of the 1,3-diol part of (*S*)-**10**, corresponding to the 1α-hydroxyl group of **1**, forms hydrogen bonds to Ser233 (OH···O: 2.79 Å) and Arg270 (OH···O: 2.94 Å). The secondary hydroxyl group of (*S*)-**10**, corresponding to the 3-hydroxyl group of **1**, interacts with Tyr143 (OH···O: 2.83 Å) and Ser274 (OH···O: 2.96 Å). The tertiary alcohol of the other alkyl chain interacts with His301 (OH···N: 2.68 Å) and His393 (OH···N: 2.94 Å), which interact with the 25-hydroxyl group of **1**.

The stereoisomer (*R*)-**10** also binds to the ligand-binding pocket of the VDR-LBD, and the overall structure of the complex is essentially similar to the active conformation induced by **1** or (*S*)-**10**. Figure 5C shows the interaction of (*R*)-**10** with the VDR-LBD. The hydroxyl groups of (*S*)-**10** and (*R*)-**10** are placed in similar positions in the two complexes, though the carbon backbones are located in slightly different positions, especially in the region of the terminal diol (Figure 5F). This conformational difference enables the hydroxyl groups with different stereochemistry to interact similarly with the same amino acid residues of the receptor. A comparison of **1** and the carborane derivatives indicates that the hydroxyl groups of these molecules are located at the same positions. On the other hand, the locations of the carbon atoms in the backbone of the carborane derivatives are considerably different from those of **1**, especially at the alkyl chain bearing two hydroxyl groups (corresponding to the A-ring) and the conjugated diene part of **1**. These results imply that the positions of the three hydroxyl groups in the carborane derivatives are adjustable to form appropriate hydrogen-bonds for VDR ligand function due to the flexible nature of the molecules.

■ DISCUSSION

We designed the unique flexible acyclic triols as a novel type of VDR ligand, focusing on the highly hydrophobic character of the icosahedral carborane cage. These flexible acyclic triols, designed as vitamin D analogs without the A-ring and conjugated diene/triene structures, exhibited potent activity, comparable to that of secosteroid **1**. Generally, an acyclic structure is entropically disadvantageous in interaction with a receptor, in comparison to a rigid cyclic structure. However, in the case of the acyclic VDR ligands developed here, flexibility of the diol moiety seems to be favorable for inducing vitamin D activity. Though (*S*)-**10** exhibited the highest potency toward HL-60 cells among the synthesized molecules, its enantiomer (*R*)-**10** also exhibited considerable activity. In addition, compound **12**, which has a 1,2-diol system, also showed moderate potency. These results contrast with the structure—activity relationship of secosteroidal compounds, in which the position and configuration of the hydroxyl groups are critical for vitamin D potency.[9] These results suggest that a suitable conformation of the two hydroxyl groups corresponding to the hydroxyl groups of **1** is induced as a consequence of the molecular flexibility of **10**.

The X-ray crystal structures revealed the molecular basis of the activity of these novel VDR ligands bearing a carborane cage, providing the first direct evidence that a carborane derivative can bind to a specific receptor protein.[22] Although the acyclic **10** exhibited relatively weak binding affinity, the X-ray structure supports the idea that **10** functions as a VDR agonist by inducing the active conformation of the receptor. In the crystal structure, the primary and secondary hydroxyl groups of the diol moiety of **10** correspond to the 1α- and 3-hydroxyl groups of **1**, respectively. It is reasonable that compound (*S*)-**10** is a more potent VDR ligand than the *R*-isomer, because (*S*)-**10** has the same stereochemistry of the secondary hydroxyl group as the 3-hydroxyl group of **1**. The fact that the difference of activity between the two enantiomers of **10** is rather small indicates that the flexible side chain can allow the two hydroxyl groups to take appropriate positions for hydrogen bonding without conformational instability. The locations of carbon atoms in the acyclic diol moiety and tethering methylene chain are rather different from the locations of the A-ring and the conjugated diene of **1**. The straight-chain backbone adopts a curvilinear conformation, and the hydroxyl groups can take suitable positions to interact with the receptor. Thus, the flexibility of acyclic triols is thought to be important for their vitamin D activity, and this is the reason why the structure—activity relationship is so different from that of secosteroids. These observations should be useful for further ligand development. A comparison with the reported crystal structure of the nonsecosteroidal VDR ligand (2*S*,2′*R*)-**5**,[23] the most potent stereoisomer of LG190178 (**5**),[24] indicates that the carborane-based VDR ligand (*S*)-**10** forms hydrogen bonds more effectively. All the hydroxyl groups of (*S*)-**10** form direct hydrogen bonds to the protein, whereas the terminal hydroxyl group of (2*S*,2′*R*)- **5** does not interact directly with the receptor. The combination of the carborane core and flexible acyclic side chain structure appears to make it easily possible for a polar substituent to take a suitable position for hydrogen-bond formation. These findings will be helpful for further development of carborane-containing bioactive molecules. Further, the finding that linear acyclic triols can function as vitamin D ligands represents a breakthrough in the development of nonsecosteroidal VDR ligands. The molecules synthesized in this study are expected to be versatile lead compounds for development of new-generation VDR ligands.

■ CONCLUSIONS

In conclusion, we have developed a novel nonsecosteroidal VDR ligand by exploiting the hydrophobicity of *p*-carborane. The novel VDR ligand exhibited potent vitamin D activity, comparable to that of the natural hormone, despite its flexible structure. X-ray crystallographic analysis revealed that the hydrophobic, spherical B—H surface of carborane could function as a

potent hydrophobic anchor in binding to the protein surface. The effective hydrophobic interaction between carborane and the receptor protein thus counteracted the entropic disadvantage of interaction of a flexible molecule. This is the first direct observation of the interaction of a boron cluster with a specific receptor protein. Our results open the way for further applications of carboranes in the field of chemical biology and medicinal chemistry

EXPERIMENTAL SECTION

Chemistry. *General Remarks.* NMR spectra were recorded on Bruker AVANCE 400 or AVANCE 500 spectrometers. Chemical shifts are reported in ppm as δ values from tetramethylsilane. Data are reported as follows: chemical shift, multiplicity (s, singlet; d, doublet; t, triplet; q quartet; br, broad; and m, multiplet), coupling constants (Hz), and integration. Mass spectra were collected on a Bruker Daltonics microTOF-2focus or JEOL AX505H in the positive and negative ion modes. Melting points were obtained on a Yanagimoto micro melting point apparatus without correction.

*1-(2-Benzyloxyethyl)-1,12-dicarba-closo-dodecaborane (**6**).* A 1.6 M solution of *n*-BuLi in *n*-hexane (9.53 mL, 15.3 mmol) was added to a solution of *p*-carborane (2.00 g, 13.9 mmol) in THF (80 mL) at 0 °C, and the mixture was stirred at room temperature for 10 min under Ar. Then, benzyl 2-bromoethyl ether (4.48 g, 20.8 mmol) was added to the mixture at 0 °C, and stirring was continued at room temperature for 16 h. The reaction mixture was poured into water and extracted with ethyl acetate. The organic layer was washed with brine, dried over sodium sulfate, and then concentrated. Purification by silica gel column chromatography (eluent; hexane) gave **6** (1.70 g, 6.11 mmol, 44%) as a white wax. ^{1}H NMR ($CDCl_3$, 400 MHz) δ 7.30−7.20 (m, 5 H), 4.39 (s, 2 H), 3.26 (t, J = 7.1 Hz, 2 H), 3.0−1.3 (br m, 10 H), 2.64 (br s, 1 H), 1.95 (t, J = 7.1 Hz, 2 H); ^{13}C NMR ($CDCl_3$, 125 MHz) δ 137.9, 128.4, 127.6, 127.5, 81.5, 72.9, 68.6, 58.5, 38.1; MS (EI+) m/z 279 [$(M - H)^+$: calcd for $C_{11}H_{21}B_{10}O$, 279].

*1-(2-Benzyloxyethyl)-12-(5-triethylsilyloxy-5-ethylheptyl)-1,12-dicarba-closo-dodecaborane (**7**).* A 1.6 M solution of *n*-BuLi in *n*-hexane (4.08 mL, 6.54 mmol) was added to a solution of **6** (1.60 g, 5.75 mmol) in THF (20 mL) at 0 °C, and the mixture was stirred at room temperature for 15 min under Ar. Then, 7-bromo-3-ethyl(3-triethylsilyloxy)-heptane (1.70 g, 5.04 mmol) was added to the mixture at 0 °C, and stirring was continued at room temperature for 40 h. The reaction mixture was poured into water and extracted with ethyl acetate. The organic layer was washed with brine, dried over sodium sulfate, and then concentrated. Purification by silica gel column chromatography (eluent; hexane/ethyl acetate, 100/1 to 20/1) gave **7** (2.60 g, 4.86 mmol, 96%) as a colorless oil. ^{1}H NMR ($CDCl_3$, 400 MHz) δ 7.31−7.25 (m, 5 H), 4.39 (s, 2 H), 3.25 (t, J = 7.1 Hz, 2 H), 3.0−1.3 (br m, 10 H), 1.95 (t, J = 7.1 Hz, 2 H), 1.60 (m, 2 H), 1.39 (q, J = 7.5 Hz, 4 H), 1.27 (m, 2 H), 1.08 (m, 4 H), 0.92 (t, J = 7.9 Hz, 9 H), 0.78 (t, J = 7.3 Hz, 6 H), 0.54 (q, J = 7.9 Hz, 6 H); ^{13}C NMR ($CDCl_3$, 125 MHz) δ 137.9, 128.4, 127.6, 127.5, 79.9, 77.9, 75.8, 72.9, 68.8, 38.3, 37.9, 36.9, 31.6, 30.2, 23.3, 8.3, 7.2, 7.0; HRMS (ESI+) m/z 559.4725 [$(M + Na)^+$: calcd for $C_{26}H_{54}B_{10}NaO_2Si$, 559.4721].

*1-(2-Hydroxyethyl)-12-(5-triethylsilyloxy-5-ethylheptyl)-1,12-dicarba-closo-dodecaborane (**8**).* A mixture of **7** (2.50 g, 4.67 mmol) and 10% palladium on carbon (250 mg) in ethanol (40 mL) and THF (5 mL) was stirred at room temperature for 3 days under atmospheric pressure of hydrogen. Insoluble materials were filtered off through Celite, and the filtrate was concentrated. Purification by silica gel column chromatography (eluent; hexane/ethyl acetate, 10/1) gave **8** (1.90 g, 91%) as a white solid. ^{1}H NMR ($CDCl_3$, 400 MHz) δ 3.44 (dt, J = 5.8 Hz, 7.0 Hz, 2 H), 3.3−1.3 (br m, 10 H), 1.89 (t, J = 7.0 Hz, 2 H), 1.61 (m, 2 H), 1.37 (q, J = 7.9 Hz, 4 H), 1.26 (m, 3 H), 1.07 (m, 4 H), 0.92 (t, J = 7.7 Hz, 9 H), 0.78 (t, J = 7.3 Hz, 6 H), 0.52 (q, J = 7.9 Hz, 6 H); ^{13}C NMR ($CDCl_3$, 125 MHz) δ 80.0, 77.9, 75.6, 61.4, 39.8, 38.3, 37.9, 31.57, 31.54, 30.2, 23.2, 8.3, 7.2, 7.0; HRMS (ESI+) m/z 469.4254 [$(M + Na)^+$: calcd for $C_{19}H_{48}B_{10}NaO_2Si$, 469.4251].

*1-{2-[(2-Phenyl-1,3-dioxan-4-yl)methoxy]ethyl}-12-(5-triethylsilyloxy-5-ethylheptyl)-1,12-dicarba-closo-dodecaborane (rac-**9**).* Compound **8** (500 mg, 1.12 mmol) was added to a suspension of sodium hydride (58 mg, 60% in oil, 1.46 mmol) in DMF (11 mL) at 0 °C, and the mixture was stirred at room temperature for 50 min under Ar. Then, 4-(*p*-toluenesulfonyloxymethyl)-2-phenyl-1,3-dioxane (1.00 g, 2.87 mmol) was added to the mixture at 0 °C, and stirring was continued at room temperature for 40 h. The reaction mixture was poured into water and extracted with ethyl acetate. The organic layer was washed with brine, dried over sodium sulfate, and then concentrated. Purification by silica gel column chromatography (eluent; hexane/ethyl acetate, 20/1 to 5/1) gave *rac*-**9** (120 mg, 0.193 mmol, 17%) as a colorless oil with 50% recovery of starting material. ^{1}H NMR ($CDCl_3$, 400 MHz) δ 7.48 (m, 2H), 7.34 (m, 3H), 5.51 (s, 1H), 4.27 (m, 1 H), 3.99 (m, 2 H), 3.50 (dd, J = 10.3 Hz, 5.9 Hz, 1 H), 3.38 (dd, J = 10.3 Hz, 4.6 Hz, 1 H), 3.3−1.3 (br m, 10 H), 3.26 (m, 2 H), 1.91 (t, J = 7.1 Hz, 2 H), 1.75−1.90 (m, 2 H), 1.58−1.49 (m, 2 H), 1.39 (q, J = 7.7 Hz, 4 H), 1.27 (m, 2 H), 1.09 (m, 4 H), 0.92 (t, J = 7.9 Hz, 9 H), 0.78 (q, J = 7.5 Hz, 6 H), 0.53 (q, J = 8.1 Hz, 6 H); ^{13}C NMR ($CDCl_3$, 125 MHz) δ 138.4, 128.8, 128.2, 126.1, 101.2, 79.9, 77.9, 76.2, 75.7, 73.6, 69.9, 66.8, 38.3, 37.9, 36.9, 31.6, 30.2, 28.0, 23.2, 8.3, 7.2, 7.0; HRMS (ESI+) m/z 645.5099 [$(M + Na)^+$: calcd for $C_{30}H_{60}B_{10}NaO_4Si$, 645.5090].

Compounds *R*-**9** and *S*-**9** were also prepared from the corresponding tosylates. All spectra data were the same as those of *rac*-**9**.

*1-[2-(2,4-Dihydroxybutoxy)ethyl]-12-(5-ethyl-5-hydroxyheptyl)-1,12-dicarba-closo-dodecaborane (rac-**10**).* Compound *rac*-**9** (100 mg, 0.161 mmol) was dissolved in methanol (4 mL) and THF (1 mL), and then 2 M hydrochloric acid (0.5 mL) was added to the solution at 0 °C. The mixture was stirred for 16 h at room temperature, poured into water, and extracted with ethyl acetate. The organic layer was washed with brine, dried over sodium sulfate, and then concentrated. Purification by silica gel column chromatography (eluent; hexane/ethyl acetate, 1/1) gave *rac*-**10** (65 mg, 0.155 mmol, 96%) as a white solid. mp 79−80 °C (*n*-hexane); ^{1}H NMR ($CDCl_3$, 400 MHz) δ 3.97 (m, 1 H), 3.84 (m, 2 H), 3.34 (dd, J = 9.2 Hz, 3.5 Hz, 1 H), 3.3−1.3 (br m, 10 H), 3.24 (m, 3H), 2.60 (d, J = 3.2 Hz, 1 H), 2.32 (t, J = 5.3 Hz, 1 H), 1.90 (t, J = 6.7 Hz, 2 H), 1.70−1.55 (m, 4 H), 1.40 (q, J = 7.5 Hz, 4 H), 1.32−1.27 (m, 2 H), 1.16−1.08 (m, 4 H), 1.00 (s, 1H), 0.82 (t, J = 7.5 Hz, 6 H); ^{13}C NMR ($CDCl_3$, 125 MHz) δ 79.9, 75.7, 74.7, 74.4, 70.1, 69.5, 61.0, 37.76, 37.73, 36.9, 34.6, 30.9, 30.0, 22.9, 7.7; HRMS (ESI+) m/z 443.3922 [$(M + Na)^+$: calcd for $C_{17}H_{42}B_{10}NaO_4$, 443.3909].

Compounds *R*-**10** and *S*-**10** were also prepared from *R*-**9** and *S*-**9**, respectively. All spectra data were the same as those of *rac*-**10**.

*1-{2-[(2,2-Dimethyl-1,3-dioxolan-4-yl)methoxy]ethyl}-12-(5-triethylsilyloxy-5-ethylheptyl)-1,12-dicarba-closo-dodecaborane (**11**).* Compound **8** (400 mg, 0.899 mmol) was added to a suspension of sodium hydride (47 mg, 60% in oil, 1.17 mmol) in DMF (10 mL) at 0 °C, and the mixture was zstirred at room temperature for 50 min under Ar. Then, 4-(*p*-toluenesulfonyloxymethyl)-2,2-dimethyl-1,3-dioxolane (500 mg, 1.74 mmol) was added to the mixture at 0 °C, and stirring was continued at room temperature for 40 h. The reaction mixture was poured into water and extracted with ethyl acetate. The organic layer was washed with brine, dried over sodium sulfate, and then concentrated. Purification by silica gel column chromatography (eluent; hexane/ethyl acetate, 20/1 to 5/1) gave **11** (230 mg, 0.401 mmol, 45%) as a colorless oil. ^{1}H NMR ($CDCl_3$, 400 MHz) δ 4.19 (m, 1 H), 4.02 (dd, J = 8.2 Hz, 6.4 Hz, 1 H), 3.69 (dd, J = 8.2 Hz, 6.4 Hz, 1 H), 3.40 (dd, J = 9.7 Hz, 5.5 Hz, 1 H), 3.33 (dd, J = 9.7 Hz, 5.5 Hz, 1 H), 3.3−1.3 (br m, 10 H), 3.22 (m, 2 H), 1.90 (t, J = 7.5 Hz, 2 H), 1.58 (m, 2 H), 1.40 (s, 3 H), 1.38 (q, J = 7.7 Hz, 4 H), 1.35 (s, 3 H), 1.27 (m, 2 H), 1.08

(m, 4 H), 0.92 (t, J = 7.7 Hz, 9 H), 0.78 (t, J = 7.5 Hz, 6 H), 0.54 (q, J = 7.9 Hz, 6 H); ^{13}C NMR ($CDCl_3$, 125 MHz) δ 109.4, 79.9, 77.9, 75.6, 74.5, 71.6, 69.9, 66.7, 38.3, 37.9, 36.7, 31.6, 30.2, 26.7, 25.4, 23.2, 8.3, 7.2, 7.0; HRMS (ESI+) m/z 583.4935 [$(M + Na)^+$: calcd for $C_{25}H_{58}B_{10}NaO_4Si$, 583.4933].

*1-[2-(2,3-Dihydroxypropoxy)ethyl]-12-(5-ethyl-5-hydroxyheptyl)-1,12-dicarba-closo-dodecaborane (**12**).* Compound **11** (200 mg, 0.349 mmol) was dissolved in methanol (6 mL) and THF (2 mL), and then 2 M hydrochloric acid (2 mL) was added to the solution at 0 °C. The mixture was stirred for 16 h at room temperature, poured into water, and extracted with ethyl acetate. The organic layer was washed with brine, dried over sodium sulfate, and then concentrated. Purification by silica gel column chromatography (eluent; hexane/ethyl acetate, 1/1) gave **12** (130 mg, 0.321 mmol, 92%) as a white solid. mp 104–105 °C (n-hexane), ^{1}H NMR ($CDCl_3$, 400 MHz) δ 3.79 (m, 1 H), 3.65 (m, 1H), 3.62 (m, 1 H), 3.42–3.36 (m, 2 H), 3.3–1.3 (br m, 10 H), 3.27–3.20 (m, 2 H), 2.46 (d, J = 5.5 Hz, 1 H), 1.99 (m, 1 H), 1.90 (t, J = 6.8 Hz, 2 H), 1.60 (m, 2 H), 1.40 (q, J = 7.5 Hz, 4 H), 1.30–1.26 (m, 2 H), 1.14–1.08 (m, 4 H), 1.00 (s, 1 H), 0.82 (t, J = 7.5 Hz, 6 H); ^{13}C NMR ($CDCl_3$, 125 MHz) δ 79.9, 75.7, 74.5, 72.2, 70.4, 69.7, 63.9, 37.76, 37.72, 36.9, 30.9, 30.0, 22.9, 7.7; HRMS (ESI+) m/z 429.3758 [$(M + Na)^+$: calcd for $C_{16}H_{40}B_{10}NaO_4$, 429.3753].

*1-(3-Hydroxypropyl)-1,12-dicarba-closo-dodecaborane (**13**).* A 1.57 M solution of n-BuLi in n-hexane (24.3 mL, 38.1 mmol) was added to a solution of p-carborane (5.00 g, 34.7 mmol) in ether (120 mL) at 0 °C, and the mixture was stirred at room temperature for 1 h. Then, trimethylene oxide (2.21 g, 38.1 mmol) was added to the mixture, and stirring was continued at room temperature for 16 h. The reaction mixture was poured into water and extracted with ether. The organic layer was washed with brine, dried over magnesium sulfate, and then concentrated. Purification by silica gel column chromatography (eluent; hexane/ethyl acetate, 8:1) gave **13** (36%) as a white solid. ^{1}H NMR ($CDCl_3$, 400 MHz) δ 3.49 (t, J = 6.3 Hz, 2 H), 3.0–1.4 (br m, 10 H), 2.66 (br s, 1 H), 1.76–1.70 (m, 2 H), 1.47–1.39 (m, 2 H); ^{13}C NMR ($CDCl_3$, 125 MHz) δ 84.1, 61.8, 58.1, 35.3, 32.2; MS (EI+) m/z 210 [$(M - H)^+$: calcd for $C_5H_{17}B_{10}O$, 201].

*1-{3-[(2,2-Dimethyl-1,3-dioxolan-4-yl)methoxy]propyl}-1,12-dicarba-closo-dodecaborane (**14**).* Compound **13** (900 mg, 4.45 mmol) was added to a suspension of sodium hydride (214 mg, 60% in oil, 5.34 mmol) in DMF (18 mL) at 0 °C, and the mixture was stirred at room temperature for 1.0 h under Ar. Then 4-(p-toluenesulfonyloxymethyl)-2,2-dimethyl-1,3-dioxolane (1.20 g, 4.19 mmol) was added to the mixture at 0 °C, and stirring was continued at room temperature for 20 h. The reaction mixture was poured into water and extracted with ethyl acetate. The organic layer was washed with brine, dried over sodium sulfate, and then concentrated. Purification by silica gel column chromatography (eluent; hexane/ethyl acetate, 10/1 to 3/1) gave **14** (350 mg, 1.11 mmol, 26%) as a colorless oil. ^{1}H NMR ($CDCl_3$, 500 MHz) δ 4.19 (m, 1 H), 4.02 (dd, J = 8.2 Hz, 6.4 Hz, 1 H), 3.69 (dd, J = 8.2 Hz, 6.4 Hz, 1 H), 3.45 (dd, J = 9.7 Hz, 5.5 Hz, 1 H), 3.38–3.26 (m, 3 H), 3.3–1.3 (br m, 10 H), 2.65 (br s, 1 H), 1.71 (m, 2 H), 1.46 (m, 1H), 1.43 (s, 3 H), 1.38 (s, 3 H); ^{13}C NMR ($CDCl_3$, 125 MHz) δ 109.4, 84.2, 74.6, 71.7, 70.5, 66.7, 58.0, 35.5, 29.3, 26.7, 25.4; HRMS (ESI+) m/z 341.2868 [$(M + Na)^+$: calcd for $C_{11}H_{28}B_{10}NaO_3$, 341.2864].

*1-{3-[(2,2-Dimethyl-1,3-dioxolan-4-yl)methoxy]propyl}-12-(5-triethylsilyloxy-5-ethylheptyl)-1,12-dicarba-closo-dodecaborane (**15**).* A 1.6 M solution of n-BuLi in n-hexane (0.900 mL, 1.43 mmol) was added to a solution of **14** (350 mg, 1.11 mmol) in THF (5 mL) at 0 °C, and the mixture was stirred at room temperature for 10 min under Ar. Then, 7-bromo-3-ethyl-(3-triethylsilyloxy)heptane (640 mg, 1.90 mmol) was added to the mixture at 0 °C, and stirring was continued at room temperature for 40 h. The reaction mixture was poured into water and extracted with ethyl acetate. The organic layer was washed with brine, dried over sodium sulfate, and then concentrated. Purification by silica gel column chromatography (eluent; hexane/ethyl acetate, 100/1 to 10/1) gave **15** (600 mg, 1.05 mmol, 94%) as a colorless oil. ^{1}H NMR ($CDCl_3$, 400 MHz) δ 4.20 (m, 1 H), 4.02 (dd, J = 8.2 Hz, 6.4 Hz, 1 H), 3.66 (dd, J = 8.2 Hz, 6.4 Hz, 1 H), 3.42 (dd, J = 9.9 Hz, 5.7 Hz, 1 H), 3.36–3.24 (m, 3 H), 3.3–1.3 (br m, 10 H), 1.70–1.65 (m, 2 H), 1.62–1.55 (m, 2 H), 1.46–1.34 (m, 6 H), 1.40 (s, 3 H), 1.35 (s, 3 H), 1.30–1.24 (m, 2 H), 1.10–1.05 (m, 4 H), 0.92 (t, J = 8.1 Hz, 9 H), 0.78 (t, J = 7.5 Hz, 6 H), 0.54 (q, J = 7.9 Hz, 6 H); ^{13}C NMR ($CDCl_3$, 125 MHz) δ 109.4, 79.4, 78.6, 77.9, 74.6, 71.7, 70.5, 66.7, 38.3, 37.9, 34.3, 31.6, 30.2, 29.4, 26.7, 25.4, 23.3, 8.3, 7.2, 7.0; HRMS (ESI+) m/z 597.5097 [$(M + Na)^+$: calcd for $C_{26}H_{60}B_{10}NaO_4Si$, 597.5089].

*1-[3-(2,3-Dihydroxypropoxy)propyl]-12-(5-ethyl-5-hydroxyheptyl)-1,12-dicarba-closo-dodecaborane (**16**).* Compound **15** (600 mg, 1.05 mmol) was dissolved in methanol (15 mL) and THF (5 mL), and then 2 M hydrochloric acid (2 mL) was added to the solution at 0 °C. The mixture was stirred for 20 h at room temperature, poured into water, and extracted with ethyl acetate. The organic layer was washed with brine, dried over sodium sulfate, and then concentrated. Purification by silica gel column chromatography (eluent; hexane/ethyl acetate, 1/1) gave **16** (310 mg, 0.741 mmol, 71%) as a white solid. ^{1}H NMR ($CDCl_3$, 400 MHz) δ 3.82 (m, 1 H), 3.69 (m, 1 H), 3.60 (m, 1 H), 3.45–3.38 (m, 2 H), 3.3–1.3 (br m, 10 H), 3.29 (t, J = 6.2 Hz, 2 H), 2.40 (d, J = 4.9 Hz, 1 H), 1.90 (dd, J = 6.8 Hz, 5.4 Hz, 1 H), 1.70–1.57 (m, 4 H), 1.45–1.37 (m, 2 H), 1.40 (q, J = 7.5 Hz, 4 H), 1.32–1.27 (m, 2 H), 1.14–1.08 (m, 4 H), 1.00 (s, 1 H), 0.82 (t, J = 7.5 Hz, 6 H); ^{13}C NMR ($CDCl_3$, 125 MHz) δ 79.3, 78.4, 74.5, 72.3, 70.48, 70.41, 64.0, 37.7, 34.3, 30.9, 30.1, 29.4, 22.9, 7.7; HRMS (ESI+) m/z 443.3916 [$(M + Na)^+$: calcd for $C_{17}H_{42}B_{10}NaO_4$, 443.3909].

Biology. *Assay of HL-60 Cell Differentiation-Inducing Activity.* HL-60 cells were cultured in RPMI-1640 medium supplemented with 5% FBS and penicillin G and streptomycin at 37 °C under 5% CO2 in air. The cells were diluted to 8.0 × 10^4 cell/mL with RPMI-1640 (5% FBS), and ethanol solution of a test compound was added to give 10^{-9} to 10^{-6} M final concentration. Control cells were treated with the same volume of ethanol alone. 1α,25(OH)$_2$D$_3$ was always assayed at the same time as a positive control. The cells were incubated at 37 °C under 5% CO_2 in air for 4 days. The percentage of differentiated cells was determined by nitro-blue tetrazolium (NBT) reduction assay. Cells were incubated at 37 °C for 20 min in RPMI-1640 (5% FBS) and an equal volume of phosphate-buffered saline (PBS) containing NBT (0.2%) and 12-O-tetradecanoylphorbol 13-acetate (TPA; 200 ng/mL). The percentage of cells containing blue-black formazan was determined in a minimum of 200 cells.

Competitive Binding Assay with Bovine Thymus VDR. Binding to bovine thymus VDR was evaluated according to the reported procedure. Bovine thymus VDR was purchased from Yamasa Biochemical (Choshi, Chiba, Japan) and dissolved in 0.05 M phosphate buffer (pH 7.4) containing 0.3 M KCl and 5 mM dithiothreitol just before use. The receptor solution (500 μL) in an assay tube was incubated with 0.072 nM [^{3}H] 1α,25(OH)$_2$D$_3$, together with graded amounts of each vitamin D analogue or vehicle for 19 h at 4 °C. Bound and free [^{3}H] 1α,25(OH)$_2$D$_3$ were separated on dextran-coated charcoal for 20 min at 4 °C. The assay tubes were centrifuged at 1000 g for 10 min. The radioactivity of the supernatant was counted, and nonspecific binding was subtracted. These experiments were done in duplicate.

X-ray Crystallographic Analysis. In this study, the method reported by Vanhooke et al. was used with some modifications to prepare the crystals of VDR complexes.[21] The rat VDR-LBD (residues 116–423, Δ165–211) was cloned as an N-terminal His$_6$-tagged fusion protein into the pET14b expression vector and overproduced in *Escherichia coli* C41. The cells were grown at 37 °C in LB medium (including ampicillin 100 mg/L) and subsequently induced for 6 h with 1S μM isopropyl-β-D-thiogalactopyranoside (IPTG) at 23 °C. The purification procedure included affinity chromatography on a Ni-NTA column, followed by dialysis and cation-exchange chromatography (SP-Sepharose). After tag removal by thrombin digestion, protease was removed by filtration

dx.doi.org/10.1021/ja208797n |J. Am. Chem. Soc. 2011, 133, 20933–20941